CO_2-to-Methanol Hydrogenation on Zirconia-Supported Copper Nanoparticles: Reaction Intermediates and the Role of the Metal–Support Interface

Kim Larmier,[a] Wei-Chih Liao,[a] Shohei Tada, [a] Erwin Lam,[a] René Vérel,[a] Atul Bansode,[b] Atsushi Urakawa,[b] Aleix Comas-Vives*[a]and Christophe Copéret*[a]

Abstract: Methanol synthesis via CO_2 hydrogenation is a key step in methanol-based economy. This reaction is catalyzed by supported copper nanoparticles and displays strong support or promoter effects. Zirconia is known to enhance both the methanol production rate and the selectivity. Nevertheless, the origin of this observation and the reaction mechanisms associated with the conversion of CO_2 to methanol still remain unknown. Here, we present a mechanistic study of the hydrogenation of CO_2 on Cu/ZrO_2. Using kinetics, *in situ* IR and NMR spectroscopies and isotopic labeling strategies, we examined the surface intermediates during CO_2 hydrogenation at different pressures. Combined with DFT calculations, we show that formate species is the reaction intermediate and that the zirconia/copper interface is a key for its conversion to methanol.

The catalytic hydrogenation of carbon dioxide to methanol is a key process in the sustainable methanol-based economy.[1] While copper-based catalysts are highly active for this transformation,[2] their activity and selectivity strongly depend on the support and/or the promoters. Understanding the copper-support interaction – its effect on the activity and product selectivity – has been a very intensive field of research over the last decade. While the reaction mechanisms and the nature of the active sites on Cu/ZnO systems have been extensively investigated,[3] copper supported on zirconia and related materials also exhibits high activity and selectivity in CO_2 hydrogenation to methanol (Eq. 1) by minimizing the formation of CO, a byproduct often resulting from the competitive reverse water-gas shift reaction (Eq. 2).[4]

$CO_2 + 3H_2 = CH_3OH + H_2O$ $\quad \Delta_rH°$ (500 K) = –62 kJ.mol^{-1} **(1)**
$CO_2 + H_2 = CO + H_2O$ $\quad \Delta_rH°$ (500 K) = +40 kJ.mol^{-1} **(2)**

Although the copper-zirconia interface was proposed to play a key role in the selective formation of methanol,[4c, 4e-g] the active site and the reaction mechanism, including the role of the interface on methanol selectivity, are still not understood. In fact, mechanistic investigations using Diffuse Reflectance IR Fourier Transform spectroscopy (DRIFTS) led to opposite conclusions: formate is an intermediate in methanol formation[4c, 4d] vs. CO_2 is first reduced to CO that is in turn hydrogenated to methanol through a carboxyl intermediate.[4f]

Herein, by using a combined experimental and computational approach on realistic models, we investigated the reaction mechanism of CO_2 hydrogenation to methanol on a Cu/ZrO_2 catalyst. Kinetic investigation, *in situ* and *ex situ* spectroscopies – FTIR and NMR – together with isotopic labeling and computational modelling showed that methanol is a primary product formed by the hydrogenation of formate as a reaction intermediate.

First, narrowly dispersed copper nanoparticles supported on monoclinic zirconia were prepared by a molecular approach.[5] Grafting of $[Cu(O^tBu)]_4$ on the surface hydroxyl groups of the support (Figure S1-S2, Scheme S1) followed by a treatment under H_2 at 500 °C for 5 h[6] yields small and narrowly distributed Cu nanoparticles: 2.2 ± 0.5 nm with 0.8 wt% Cu loading (Figure S3a). We also prepared via the same method a Cu/SiO_2 catalyst as a prototype of pure copper particles in order to probe their specific reactivity. This sample contains Cu particles with a size distribution of 2.1 ± 0.5 nm for 2.3 % of Cu loading (Figure S3b). Their catalytic activities were measured in a fixed-bed flow reactor at 230 °C and 25 bars (H_2/CO_2 molar ratio 3:1) under steady-state conditions (Figure S4). For each sample, the contact time was increased by decreasing the volumetric flow rate *Q* of the feed gas. Figure 1a shows the evolution of the formation rates of methanol and CO as a function of the contact time. For both catalysts, the rates strongly depend on the contact time. Extrapolation of the initial rates to zero conversion (zero contact time) for the two catalysts (Figure 1b) clearly show a strictly positive initial rate of formation for both CO and methanol, which indicates that they are both primary products. Thus, the intermediacy of CO in the formation of methanol is unlikely. Second, while the rate of CO formation is of the same order of magnitude on both catalysts, the rate of methanol formation is dramatically increased on Cu/ZrO_2. Thus, CO formation likely occurs on the Cu surface, while methanol is formed at a much higher rate when both copper and zirconia are present. As a result, Cu/ZrO_2 displays much higher initial activity and methanol selectivity (15 μmol.s^{-1}.g_{Cu}^{-1}, 75 %) than Cu/SiO_2 (2.6 μmol.s^{-1}.g_{Cu}^{-1}, 50 %). On Cu/SiO_2, the rate of CO formation increases with contact time while the opposite is observed for methanol, which is likely due to partial methanol decomposition into CO. On Cu/ZrO_2, similar trends are observed for CO formation. However, the decrease in methanol formation rate with contact time is much sharper, which is likely due to inhibition of methanol formation by reaction products, such as water or methanol itself. Both molecules are basic and strongly bind ZrO_2, suggesting that the active sites may involve Lewis acidic Zr atoms. This inhibition is essentially reversible as going

[a] Dr K. Larmier, Mr. W.-C. Liao, Dr. S. Tada, Mr. E. Lam, Dr. R. Vérel, Dr. A. Comas-Vives, Prof. C. Copéret
Department of Chemistry and Applied Biosciences
ETH Zürich
Vladimir-Prelog Weg 1-5, CH-8093 Zürich, Switzerland
E-mail: comas@inorg.chem.ethz.ch
E-mail: ccoperet@inorg.chem.ethz.ch
[b] Dr. A. Bansode, Prof. A. Urakawa
Institute of Chemical Research of Catalonia (ICIQ),
The Barcelona Institute of Science and Technology,
Av. Països Catalans 16, 43007 Tarragona, Spain
E-mail: aurakawa@iciq.es

This work was presented at the CO_2 Catalysis Conference , April 2016, Albufeira, Portugal

Supporting information for this article is given via a link at the end of the document.

back to a low contact time mostly restores the activity. A slight deactivation occurs over 40 h on stream (empty data point in Fig. 1a). Overall, the methanol selectivity strongly decreases with contact time and conversion on both catalysts (Figure S4c-d).

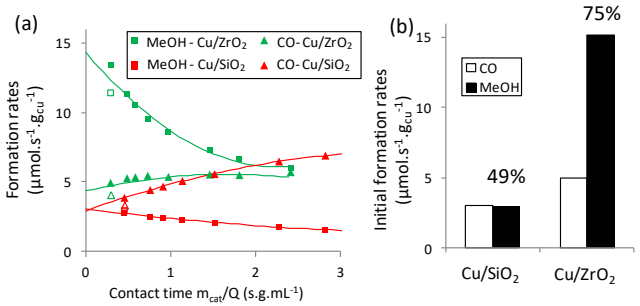

Figure 1. (a) Evolution of the rate of formation of CO and methanol with contact time on Cu/ZrO_2 and Cu/SiO_2 measured in a flow reactor at 230 °C and 25 bars (H_2/CO_2 = 3:1). The empty points show the activity when the first data point was repeated after 40 h of reaction, showing slow deactivation. CO_2 conversion was kept between 0.5 and 6 %. (b) Extrapolated rates of formation at zero conversion. The selectivity to methanol is indicated.

In order to obtain information about surface reaction intermediates, CO_2 hydrogenation on Cu/ZrO_2 was investigated by *in situ* DRIFTS at 230 °C under varying pressures (1-20 bars). The IR spectrum of the pristine catalyst shows only OH stretching frequencies at 3774 and 3670 cm^{-1} (Figure S5a). After contacting pre-reduced Cu/ZrO_2 with H_2/CO_2 mixture (3:1) at 230 °C and 1 bar, features appeared in the ν-CH (Figure S6a) and ν-CO regions (Figure S6b). The main broad ν-OCO features at 1593 cm^{-1} can be attributed to carbonate or bicarbonate (CO_3* or (CO_3H*),[7] and the bands at 2978, 2878, 2736, 1567 and 1387 cm^{-1} are characteristic of formate species adsorbed on zirconia ($HCOO\_ZrO_2$, ESI Section 5).[4d, 7-8] The presence of formate on copper cannot be excluded as a characteristic band at 1357 cm^{-1} is also observed.[4d] Increasing the reaction pressure to 5 bars (Figure S6a-b) or higher pressures resulted in the appearance of new features at 2942, 2828 cm^{-1} and the characteristic C-O stretching frequencies at 1154 and 1049 cm^{-1} that were attributed to methoxy adsorbed on zirconia.[4f, 7] Interestingly, when pure ZrO_2 was used, only carbonate, bicarbonate and formate species were observed (Figure S6). This suggests that the presence of Cu on ZrO_2 is responsible for the formation of methoxy species.

We subsequently investigated the nature of the reaction intermediates by solid-state NMR spectroscopy. Note that NMR will preferably provide information about species adsorbed on zirconia, as adsorbed species on metallic copper will suffer from signal broadening and disappearance (ESI, Section 5). Cu/ZrO_2 was contacted with a $H_2/^{13}CO_2$ mixture (3:1) at 230 °C for 12 h in a high-pressure glass reactor at 1 and 5 bars, respectively. After cooling down to room temperature, the gas phase was evacuated and the solid was analyzed by solid-state NMR. The ^1H-^{13}C heteronuclear correlation (HETCOR) spectrum of the sample after reaction at 1 bar is shown in Figure 2a. The correlation of the ^{13}C NMR chemical shift at 168 ppm to the ^1H NMR signal at 8.4 ppm is consistent with the presence of formate species; the line broadening in the ^1H dimension suggests the presence of formate in different chemical environments. After reaction at 5 bars (Figure 2b), an additional correlation is observed at $\delta(^{13}C)$ = 51 ppm and $\delta(^1H)$ = 4.0 ppm consistent with the formation of surface methoxy species. The NMR data are in agreement with what is observed by *in situ* DRIFTS. However, the absence of carbonates in both, *ex situ* NMR or IR experiments (Figure S5b-c) shows that these species are weakly adsorbed.

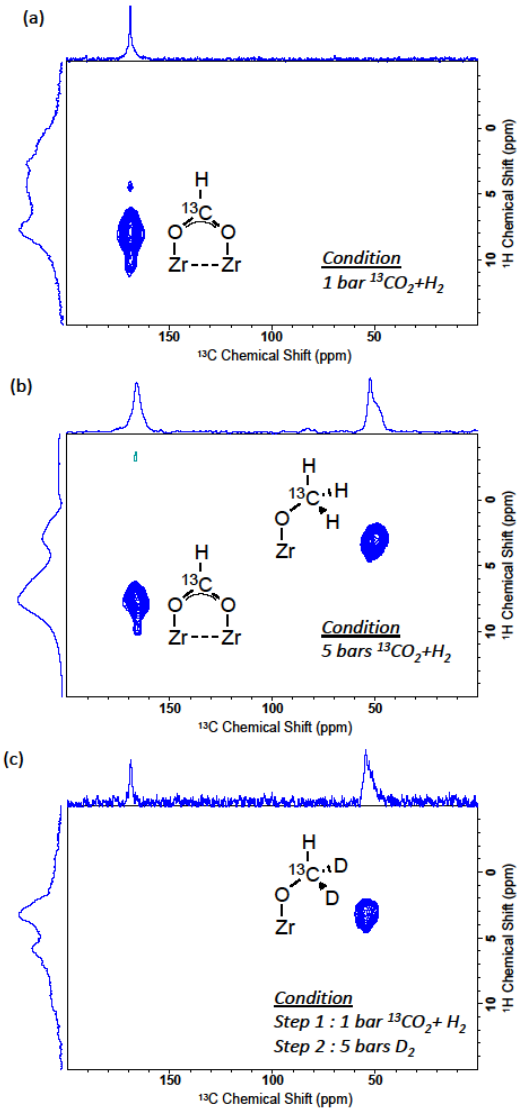

Figure 2. *Ex situ* MAS-NMR ^{1}H-^{13}C HETCOR spectra of Cu/ZrO_2 reacted with $H_2/^{13}CO_2$ (3:1) at 230 °C for 12 h at **(a)** 1 bar or **(b)** 5 bars. **(c)** *Ex situ* MAS-NMR ^{1}H-^{13}C HETCOR spectrum of Cu/ZrO_2 after two step hydrogenation of $^{13}CO_2$: (1) hydrogenation at 1bar, 230 °C, 12h (2) deuteration at 5 bars, 230 °C, 12h . For HETCOR experiments, ramp cross polarization (^{1}H-^{13}C) was used with contact time of 0.5 ms. The recycle delay was 1 s. External projections of the 1D ^{13}C and ^{1}H spectra are applied in all spectra.

On the contrary, the formate and methoxy species are strongly adsorbed and remain on the surface even after evacuation under high vacuum. Finally, when the similar experiments were performed on pure ZrO_2, formate species were observed (Figure S16) but no methoxy, as previously observed by *in situ* DRIFTS. On Cu/SiO_2, IR shows (Figure S13) the formation of formate identified by bands at 2937, 2858, and 1544 cm^{-1} associated to a very broad and weak feature at 168 ppm in CP-MAS, and no methoxy could be observed (Figure S14-S15). Thus, copper particles by themselves or the pure support are not able to generate significant amounts of methoxy from formate under these conditions (230 °C; 5 bars).

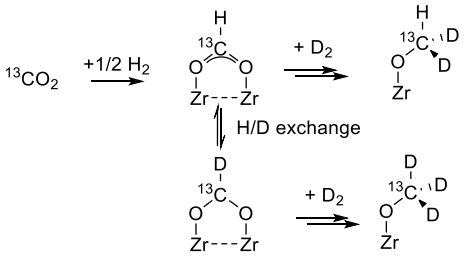

Scheme 1. Reaction scheme derived from the spectroscopic measurements.

In order to evaluate whether or not formate is a reaction intermediate towards methanol synthesis, additional isotopic labeling experiments were carried out. First, we selectively prepared ^{13}C labeled formate adsorbed on the surface ($H^{13}COO^*$) by reacting Cu/ZrO_2 with a $H_2/^{13}CO_2$ mixture (3:1) at 1 bar and 230 °C (Figure 2a). In a second step, following cooling down to room temperature and evacuation of the gas phase (10^{-4} mbar, 2 h), the sample was treated with 5 bars of D_2 at 230 °C for 12 h. MAS-NMR and IR spectra of the resulting solid were recorded (Figure 2c and S5d). ^1H-^{13}C CP-MAS NMR spectrum shows two signals at 168 and 51 ppm, attributed to formate and methoxy species, respectively. In this experiment, the formate initially present on the surface after the first step (treatment by $^{13}CO_2$ and H_2) is the only source of ^{13}C and ^1H, so that the methoxy surface species must be formed from deuteration of the initial formate species, supporting its involvement as a reaction intermediate to methanol formation. In order to further characterize the nature of the intermediates adsorbed on the surface, and the isotopic source of the methoxy species, the sample was extracted and analyzed by solution NMR; it was first divided in two fractions prior to extraction. The first fraction was extracted with D_2O and a ^1H solution NMR spectrum was recorded (Figure S18), and the second fraction was extracted with H_2O and a ^2D solution NMR spectrum was recorded (Figure S19). The ^1H spectrum shows a doublet of pentet centered at 3.12 ppm, with coupling constants $J(^1H$-$^{13}C)$ = 141 Hz and $J(^1H$-$^2D)$ of 1.7 Hz, consistent with the formation of $^{13}CHD_2OD$. The ^2D spectrum shows a doublet centered at 3.15 ppm ($J(^2D$-$^{13}C)$ = 21 Hz), but did not show additional ^1H-^2D coupling, thus showing that the most abundant species correspond to fully deuterated methanol $^{13}CD_3OH$. This is also consistent with the absence of formate signal in the ^1H-^{13}C HETCOR spectrum (Figure 2e). Taken together, the results suggest that the formate can exchange its hydrogen with deuterium prior to its subsequent deuteration, indicating that the formation of methoxy species is slower than the H/D exchange of formate as shown in Scheme 1. IR spectroscopy also reveals a high degree of H/D exchange upon contact of the sample with D_2 (Figure S5d). Nonetheless, quantitative ^{13}C direct excitation NMR spectrum (Figure S17) showed that a significant proportion of formate (deuterated or not) was converted into methoxy (about 60 %). Furthermore, the 2D spectrum in solution allowed a rough estimation of the number of methanol adsorbed on the surface prior desorption to about 0.04 par nm^{-2}, which may be considered as an indication of the number of active sites. This number is close to the density of particles that can be estimated (0.01 per nm^{-2}) indicating a rather small number of active sites per copper particle (details in ESI). The NMR spectroscopic investigation shows that methoxy (methanol) is formed from formate species adsorbed on zirconia, as proposed earlier.[4d] It also highlights the determining effect of pressure in the formation of the intermediates. We also show that both copper and zirconia are required for the reaction under such conditions. Thus, it can be proposed that the reaction takes place at the interface between zirconia and copper particles, as suggested in previous reports.[4b, 4e].

In order to get molecular insights into the reaction mechanisms and possible involvement of this interface, we turned to DFT calculations. A model for the supported copper particles on ZrO_2 and the potential interfacial active sites was constructed by depositing a Cu_{38} particle (ø = 0.8 nm, truncated octahedron from *fcc* structure) on a m-ZrO_2 ($\bar{1}11$) slab, which is the main termination exposed by monoclinic zirconia (Figure S20).[9] No significant deformation of the cluster was observed, consistent with the small change in the cohesive energy of the Cu nanoparticle upon adsorption (–266 and –269 $kJ.mol^{-1}$ prior and after adsorption, respectively). The ZrO_2 slab model and a pristine (111) surface of *fcc* copper were also used for comparison. The adsorption modes of H_2 and CO_2 were assessed on these three model materials. In line with previous findings, the dissociative adsorption of H_2 is endoenergetic on the zirconia surface, either through heterolytic (Δ_rE = +57 $kJ.mol^{-1}$) or homolytic cleavage (Δ_rE = +241 $kJ.mol^{-1}$),[9] while the dissociation of H_2 is exoenergetic by –40 $kJ.mol^{-1}$ on the Cu (111) facet.[10] On the supported nanoparticle, the dissociation is slightly more favorable than on the extended surface (Δ_rE = –50 $kJ.mol^{-1}$). CO_2 virtually does not bind the Cu (111) surface (–2 $kJ.mol^{-1}$, Figure 3a). On ZrO_2, CO_2 adsorbs as a carbonate, or bicarbonate if a hydroxyl group is available, with adsorption energies of –65 and –70 $kJ.mol^{-1}$, respectively (Figure 3b and S21). However, we found a much more favorable adsorption mode of CO_2 at the interface between copper and zirconia (Δ_rE = –179 $kJ.mol^{-1}$, Figure 3c), where CO_2 adopts a bent structure with the carbon atom bound to the copper particle surface, and the two oxygen atoms interact with Zr^{4+} Lewis acidic centers of the zirconia surface. A similar adsorption mode has been found for the adsorption of CO_2 on Ni/γ–Al_2O_3 interface.[11] Bader charge analysis of this intermediate revealed a transfer of electron density from the copper particle to the CO_2 molecule (-1.1 compared to about 0 for CO_2 on Cu(111) and carbonates on ZrO_2), which is thus negatively charged and partially reduced. The positive charge is delocalized on the copper particle. This adsorption mode of CO_2 at the Cu/ZrO_2 interface is therefore a very good candidate for further reduction by H_2, and was used as a starting point to calculate hydrogenation pathways.

We first examined the transformation of CO_2 into three intermediates commonly proposed:[3a, 12] i) direct decomposition of CO_2 into CO (first step of the reverse water-gas-shift reaction, Figure 3d), ii) carboxyl intermediate (COOH*, Figure 3e) and iii) formate intermediate (HCOO*, Figure 3f). The activation barriers to form these intermediates from CO_2 chemisorbed at the interface and H_2 dissociated on the particle are given in Figures 3d-f. Formation of the formate intermediate is the lowest energy pathway from all those evaluated, with an activation barrier of only 74 $kJ.mol^{-1}$, compared to 119 and 193 $kJ.mol^{-1}$ for the formation of CO and COOH*, respectively. It is also the most thermodynamically favorable one (–67 $kJ.mol^{-1}$) in comparison with the formation of CO and COOH* which are endoenergetic by 54 and 67 $kJ.mol^{-1}$, respectively. The whole pathway leading from CO_2 to methanol was thus calculated through the most favorable formate intermediate. The resulting energy and Gibbs free energy diagrams are depicted in Figure 4, along with the main intermediates. Note that the highest point in the free energy diagram (19 $kJ.mol^{-1}$) lies lower than the transition states for the initial activation of CO_2 to CO* (50 $kJ.mol^{-1}$) or COOH* (124 $kJ.mol^{-1}$), confirming the relevance of the formate route as the most favorable pathway. From the formate, adsorbed on ZrO_2 in close vicinity to the Cu particle, transfer of an additional hydrogen atom from the Cu particle can generate an acetal-like species $H_2C(O)_2$*, where both oxygen atoms are bound to two Zr^{4+} sites, with a low free energy barrier (71 $kJ.mol^{-1}$). The further hydrogenation of the acetal is the most energetically demanding step. A hydrogen atom is first transferred to one of the oxygen atoms to form H_2COOH^* ($\Delta_rG^‡$ = 105 $kJ.mol^{-1}$). Note however that the relative energy barrier for this step is lower than the formation of CO* and COOH* intermediates. This high-energy intermediate is easily converted by the transfer of an additional hydrogen atom ($\Delta_rG^‡$

= 52 kJ.mol^{-1}). In a concerted, S_N2-like step, the third C-H bond is formed while the C-OH bond is broken, leading to methoxy and hydroxyl groups adsorbed on the formally Zr^{4+} sites. Both can then further undergo protonation by hydrogen-transfer from the copper particle. Methanol, and water are thus formed ($\Delta_rG^{\ddagger}$ = 52 and 102 kJ.mol^{-1}, respectively), and desorb with a desorption energy of –84 and –87 kJ.mol^{-1}, respectively.

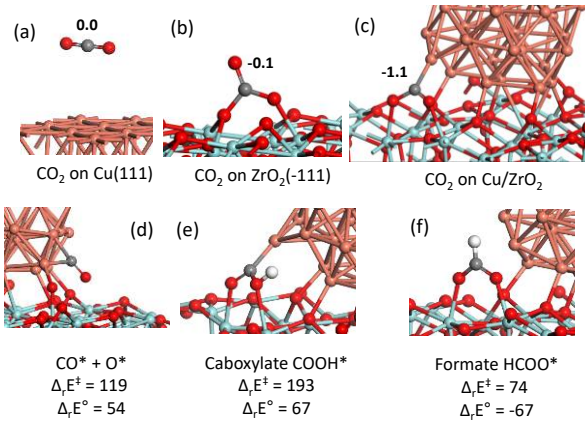

Figure 3. (a)-(c) Optimized structures of CO_2 adsorbed (a) on Cu (111) (b) on m-ZrO_2 ($\bar{1}11$) (c) at the interface between copper and zirconia. Bader charge on the CO_2 molecule are indicated. **(d)-(f)** Structures of the possible intermediates at the interface between copper and zirconia (d) CO* and O* (e) COOH* (f) formate. Activation barriers and formation enthalpy from adsorbed CO_2 + H_2 are given in kJ.mol^{-1}. Cyan: zirconium, red: oxygen, orange: copper, Grey: carbon, white: hydrogen.

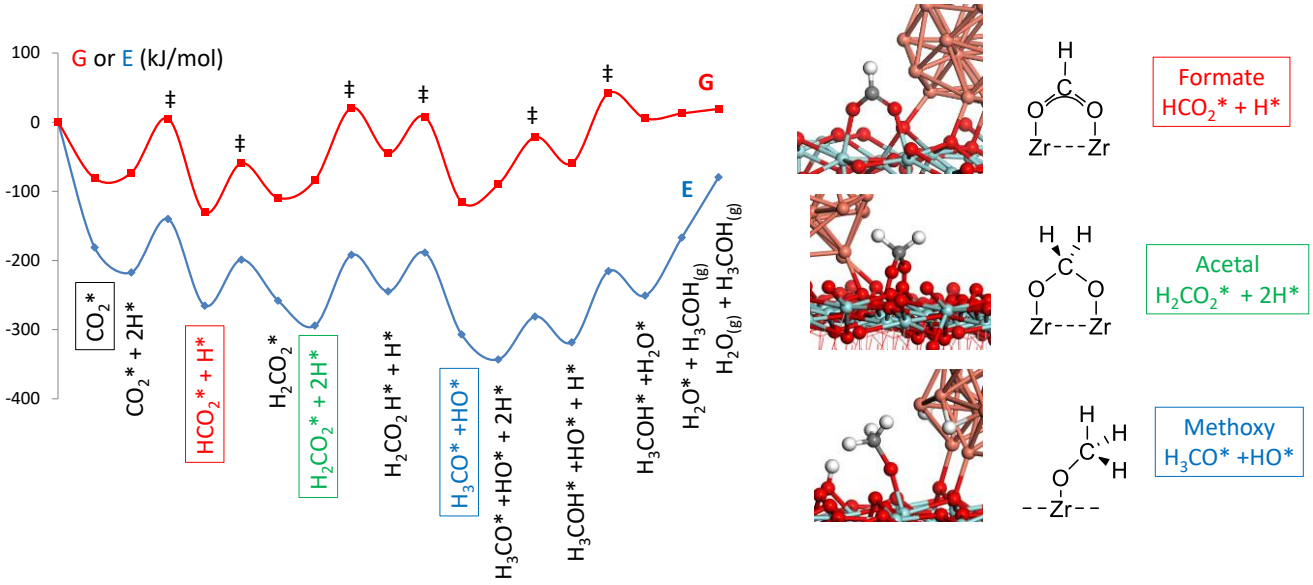

Figure 4. Energy and Standard Gibbs free energy pathway at 473 K calculated for the hydrogenation of CO_2 to methanol at the copper-zirconia interface The energetics are referenced to the Cu/ZrO_2 model and $CO_{2,(g)}$ + 3 $H_{2,(g)}$. The lowest intermediates in Gibbs free energy are shown on the right

The lowest points in the diagram are formate and methoxy, and the calculated ^{13}C and ^{1}H chemical shifts are in good agreement with the experimental data (Table S1 and Figure S22). Overall, the Gibbs free energy diagram is rather flat, with an energy span of 151 kJ.mol^{-1}. It is worth mentioning that it is significantly lower than what is found on a flat Cu(111) surface (267 kJ.mol^{-1}, Figure S23) or even stepped Cu(211) facets (over 200 kJ.mol^{-1} calculated at the GGA-PBE level of theory). [3a]

In conclusion, we show that CO_2 can be transformed into carbonate or bicarbonate, formate, methoxy, upon adsorption and hydrogenation on zirconia-supported Cu nanoparticles. Experimentally, carbonate and bicarbonate can only be observed under *in situ* conditions, consistent with the low calculated adsorption energies (about –70 kJ.mol^{-1}), in contrast with the strong adsorption of formate and methoxy species. The acetal, which is the next most stable intermediate, was not observed under the described reaction conditions. In fact, calculations show that it lies about 20 kJ.mol^{-1} higher in energy than the formate, with a low formate-acetal interconversion barrier of about 70 kJ.mol^{-1}. Thus both intermediates can be in equilibrium (in favour of the formate). This interconversion is consistent with the observed H/D exchange of the formate intermediate (Scheme 1). Overall, the formate species is a key and observable reaction intermediate in the hydrogenation of CO_2 to methanol on Cu/ZrO_2. The proposed mechanism is reminiscent to this recently proposed for Ru-molecular catalyst, bridging the gap between molecular catalysis and heterogeneous catalysis.[13] The obtained results clearly point out to the crucial molecular role of the interface between the copper particles and zirconia,[4b, 4e] paving the road toward a more rational design of efficient heterogeneous CO_2 hydrogenation catalysts.

Acknowledgements

K.L., E.L. and S.T. were supported by the SCCER – Heat and Energy Storage program, W.C.L by SNF (200020_149704), and A.C.V. by the SNF funding program (Ambizzione Project PZ00P2_148059). K.L. thanks the ETH Career Seed Grant SEED-21 16-2. S. T. also thanks the Japan Society for the Promotion of Science for a fellowship (JSPS, No. 15J10157). A.B. and A.U. acknowledge MINECO, Spain for financial support (CTQ2012-34153) and for support through Severo Ochoa Excellence Accreditation 2014–2018 (SEV-2013-0319). The authors thank Dr. T.C. Ong (ETHZ) for many useful discussions and the quantitative ^{13}C SSNMR measurement, T.-H. Lin (ETHZ) for his precious help in using the high-pressure glass-reactor, and Juan José Corral (ICIQ) for assistance during high-pressure DRIFTS measurements.

Keywords: CO_2 hydrogenation, solid-state NMR, *in situ* DRIFTS, DFT, copper, zirconia

[1] A. Goeppert, M. Czaun, J. P. Jones, G. K. S. Prakash, G. A. Olah, *Chem. Soc. Rev.* **2014**, *43*, 7995-8048.
[2] M. Saito, T. Fujitani, M. Takeuchi, T. Watanabe, *Applied Catalysis a-General* **1996**, *138*, 311-318.
[3] a) M. Behrens, F. Studt, I. Kasatkin, S. Kuhl, M. Havecker, F. Abild-Pedersen, S. Zander, F. Girgsdies, P. Kurr, B. L. Kniep, M. Tovar, R. W. Fischer, J. K. Norskov, R. Schlogl, *Science* **2012**, *336*, 893-897; b) S. Kuld, M. Thorhauge, H. Falsig, C. F. Elkjaer, S. Helveg, I. Chorkendorff, J. Sehested, *Science* **2016**, *352*, 969-974; c) T. Lunkenbein, J. Schumann, M. Behrens, R. Schlogl, M. G. Willinger, *Angew. Chem. Int. Ed.* **2015**, *54*, 4544-4548; d) F. Studt, M. Behrens, E. L. Kunkes, N. Thomas, S. Zander, A. Tarasov, J. Schumann, E. Frei, J. B. Varley, F. Abild-Pedersen, J. K. Norskov, R. Schlogl, *ChemCatChem* **2015**, *7*, 1105-1111; e) S. Zander, E. L. Kunkes, M. E. Schuster, J. Schumann, G. Weinberg, D. Teschner, N. Jacobsen, R. Schlogl, M. Behrens, *Angew. Chem. Int. Ed.* **2013**, *52*, 6536-6540; f) S. Kuld, C. Conradsen, P. G. Moses, I. Chorkendorff, J. Sehested, *Angew. Chem. Int. Ed.* **2014**, *53*, 5941-5945.
[4] a) T. Witoo, J. Chalorngtham, P. Dumrongbunditkul, M. Chareonpanich, J. Limtrakul, *Chem. Eng. J.* **2016**, *293*, 327-336; b) F. Frusteri, G. Bonura, C. Cannilla, G. D. Ferrante, A. Aloise, E. Catizzone, M. Migliori, G. Giordano, *Applied Catalysis B-Environmental* **2015**, *176*, 522-531; c) I. A. Fisher, H. C. Woo, A. T. Bell, *Catal. Lett.* **1997**, *44*, 11-17; d) I. A. Fisher, A. T. Bell, *J. Catal.* **1997**, *172*, 222-237; e) F. Arena, G. Italiano, K. Barbera, S. Bordiga, G. Bonura, L. Spadaro, F. Frusteri, *Applied Catalysis A-General* **2008**, *350*, 16-23; f) S. Kattel, B. Yan, Y. Yang, J. G. Chen, P. Liu, *The Journal of the American Chemical Society* **2016**, *138*, 12440-12450; g) I. Ro, Y. Liu, M. R. Ball, D. H. K. Jackson, J. P. Chada, C. Sener, T. F. Kuech, R. J. Madon, G. W. Huber, J. A. Dumesic, *ACS Cat.* **2016**, *6*, 7040-7050.
[5] C. Coperet, A. Comas-Vives, M. P. Conley, D. P. Estes, A. Fedorov, V. Mougel, H. Nagae, F. Nunez-Zarur, P. A. Zhizhko, *Chem. Rev.* **2016**, *116*, 323-421.
[6] A. Roussey, P. Gentile, D. Lafond, E. Martinez, V. Jousseaume, C. Thieuleux, C. Coperet, *J. Mat. Chem. C* **2013**, *1*, 1583-1587.
[7] E. Guglielminotti, *Langmuir* **1990**, *6*, 1455-1460.
[8] F. Ouyang, J. N. Kondo, K. Maruya, K. Domen, *Catal. Lett.* **1998**, *50*, 179-181.
[9] a) O. Syzgantseva, M. Calatayud, C. Minot, *J. Phys. Chem. C.* **2010**, *114*, 11918-11923; b) O. A. Syzgantseva, M. Calatayud, C. Minot, *J. Phys. Chem. C.* **2012**, *116*, 6636-6644.
[10] a) K. Mudiyanselage, Y. X. Yang, F. M. Hoffmann, O. J. Furlong, J. Hrbek, M. G. White, P. Liu, D. J. Stacchiola, *J. Chem. Phys.* **2013**, *139*; b) E. M. Mccash, S. F. Parker, J. Pritchard, M. A. Chesters, *Surf. Sci.* **1989**, *215*, 363-377.
[11] M.-C. Silaghi, A. Comas-Vives, C. Copéret, *ACS Cat.* **2016**, *6*, 4501-4505.
[12] a) Y. Yang, D. H. Mei, C. H. F. Peden, C. T. Campbell, C. A. Mims, *ACS Cat.* **2015**, *5*, 7328-7337; b) Q. L. Tang, Z. P. Liu, *J. Phys. Chem. C.* **2010**, *114*, 8423-8430; c) J. Graciani, K. Mudiyanselage, F. Xu, A. E. Baber, J. Evans, S. D. Senanayake, D. J. Stacchiola, P. Liu, J. Hrbek, J. F. Sanz, J. A. Rodriguez, *Science* **2014**, *345*, 546-550; d) M. D. Marcinkowski, C. J. Murphy, M. L. Liriano, N. A. Wasio, F. R. Lucci, E. C. H. Sykes, *ACS Cat.* **2015**, *5*, 7371-7378.
[13] S. Wesselbaum, V. Moha, M. Meuresch, S. Brosinski, K. M. Thenert, J. Kothe, T. V. Stein, U. Englert, M. Holscher, J. Klankermayer, W. Leitner, *Chem. Sci.* **2015**, *6*, 693-704.

Supporting Information

Reaction Intermediates and Role of the Interface in the CO_2 hydrogenation to CH_3OH on ZrO_2-supported Cu Nanoparticles

Kim Larmier,[a] Wei-Chih Liao,[a] Shohei Tada,[a] Erwin Lam,[a] René Vérel,[a] Atul Bansode,[b] Atsushi Urakawa,[b] Aleix Comas-Vives,[a] Christophe Copéret[a]**

[a] ETH Zürich, Department of Chemistry and Applied Biosciences, Vladimir-Prelog Weg 2, CH-8093 Zürich, Switzerland

[b] Institute of Chemical Research of Catalonia (ICIQ), The Barcelona Institute of Science and Technology, Av. Països Catalans 16, 43007 Tarragona, Spain

* Corresponding author: comas@inorg.chem.ethz.ch, ccoperet@inorg.chem.ethz.ch

1. Methods

Experimental.

pXRD – Powder XRD patterns were recorded on a STOE STADI P apparatus at a voltage of 40 kV and a current of 35 mA.

N_2 physisorption – The specific surface area of the support was measured from a nitrogen physisorption isotherm recorded at 77 K on a BEL JAPAN BELSORP-min apparatus. The data were analyzed by the BET method.

TEM – The morphology of the samples was obtained by transmission electron microscopy (TEM, Philips CM12) and by high resolution TEM (FEI Tecnai F30).

Fourier-Transform InfraRed spectroscopy - FTIR measurements were carried out on a Bruker Alfa-T spectrometer (inside a glovebox under Ar atmosphere). The powdered samples were pressed into a thin disk using a 7 mm die set. Typically, 24 scans were collected for each spectrum at a resolution of 4 cm^{-1}. Background spectra were collected under Ar atmosphere.

In situ DRIFTS (Diffuse Reflectance Infrared Fourier Transform Spectroscopy) – In situ DRIFTS measurements were performed in a custom-made high-pressure reaction cell having a cylindrical cavity (3 mm in diameter and 3 mm vertical length) for the sample placement. The cell, resembling that reported previously,[1] was mounted in a Praying Mantis (Harrick) optical accessory. Approximately, 10-15 mg of catalyst powder was placed in the cell and reduced at 250 °C for 1 h under continuous flow of H_2 (15 $mL \cdot min^{-1}$), prior to the exposure to the reaction gas mixture (CO_2:H_2 = 1:3). For the measurements under ambient pressure conditions, a continuous flow of the gas mixture was passed over the catalyst at 15 $mL \cdot min^{-1}$. For the experiments, involving reaction pressure up to 20 bars, a high-pressure needle valve was placed at the outlet of cell to build the pressure in the cell. The flow of the gas mixture was stopped after attaining the desired reaction pressure. The spectra were collected with 4 cm^{-1} resolution on an FT-IR spectrometer (TENSOR 27 / Vertex 70, Bruker) equipped with a liquid-nitrogen-cooled MCT detector. The DRIFT spectrum recorded under H_2 flow at the reaction temperature was used as the background.

NMR spectroscopy –

The solution NMR experiments were done on a Bruker 500 MHz AVANCE III HD spectrometer with a 5 mm probe. The chemical shifts were referenced to the residual proton in the solvent.

The solid-state NMR experiments were done in a Bruker 400 MHz AVANCE III HD spectrometer with a 4 mm MAS triple resonance probe operating in double resonance mode. The MAS frequency was set to 10 kHz. The chemical shift scale was calibrated using admantane as an external secondary reference. Ramped cross polarization (^1H-^{13}C) was used for most experiments with ^1H excitation frequency ($\gamma\beta_1$) at 100 kHz. The contact time was 2 ms for 1D experiments and 0.5 ms for ^1H-^{13}C HETCOR experiments. Additionally, for ^1H-^{13}C HETCOR experiment, DUMBO homonuclear (^1H-^1H) decoupling was used during t_1.[2]

Ab initio calculations.

Periodic DFT calculations were carried out with Vienna Ab Initio Simulation Package (VASP)[3] code using the projector augmented wave (PAW) method[4] with a plane wave energy cutoff of 400 eV and the PBE exchange-correlation functional. The criterion convergence chosen for the SCF cycle was 10^{-5} eV, and optimizations were considered converged once the forces on all atoms were lower than 0.1 $eV.Å^{-1}$.

To model the zirconia surface, we considered a slab of the ($\bar{1}11$) termination of monoclinic zirconia. The slab was 13.6 x 14.7 Å large, and 9 Å thick (144 atoms, 48 ZrO_2 units), with a vacuum separation of 17 Å. The three lowest atomic layers were frozen during optimizations and transition state calculations. The Brillouin zone was sampled with a 2 x 2 x 1 k-point grid.

Electron occupancies were determined according to a gaussian scheme with an energy smearing of 0.1 eV. For the supported copper particle, a Cu_{38} cluster of truncated octahedron shape from Cu *fcc* structure was deposited on the surface. The ensemble was optimized before studying the adsorption and reactivity of CO_2 and H_2.

Cu(111) was simulated using a periodic 3 x 3 four-layer slab consisting of 36 Cu atoms with a vacuum separation of 15 Å. During optimization the first Cu(111) layer was kept frozen. The Brillouin zone was sampled with a 3 x 3 x 1 k-point grid. Electron occupancies were determined according to a Methfessel-Paxton scheme with an energy smearing of 0.2 eV.

Transition states were determined using the Climbing Image Nudge Elastic Band (Cl-NEB) method with 8 images.[5] The transition states were confirmed by frequency analysis.

Chemical shifts calculations were performed using the linear response method implemented in VASP. For these calculations, the convergence criterion on the SCF cycles was set to 10^{-8} eV.

Thermodynamic calculations including enthalpic and entropic corrections were performed to calculate the Gibbs free energies by calculating the vibration frequencies for the gas-phase molecules, the adsorbed species and the transition states. The procedure used in this publication is fully described in Larmier et al [6] :

For a given species *i*, G(*i*,T,P) can be calculated through the formula **(S1)**

$$G(i,T,P) = E(i) + U_{vib}(i,T) + U_{rot}(i,T) + U_{trans}(i,T) + PV_m - T \times S_{vib}(i,T) - T \times S_{rot}(i,T) - T \times S_{trans}(i,T,P) \quad \textbf{(S1)}$$

The vibrational, rotational and translational enthalpic and entropic contributions for a gas phase molecule considered as an ideal gas can be calculated with equations **(S2) – (S8)**:

$$U_{vib}(i,T) = N_A \left[\sum_n \frac{1}{2} h\nu_n + \sum_n \frac{h\nu_n \times \exp\left(-\frac{h\nu_n}{k_B T}\right)}{1 - \exp\left(-\frac{h\nu_n}{k_B T}\right)} \right] \quad \textbf{(S2)}$$

$$U_{trans}(i,T) + U_{rot}(i,T) + PV_m(i,T) = 4RT \text{ (non-linear molecules)} \quad \textbf{(S3)}$$

$$U_{trans}(i,T) + U_{rot}(i,T) + PV_m(i,T) = 7/2RT \text{ (linear molecules)} \quad \textbf{(S4)}$$

$$S_{vib}(i,T) = N_A k_B \left[\sum_n \frac{\frac{h\nu_n}{k_B T} \times \exp\left(-\frac{h\nu_n}{k_B T}\right)}{1 - \exp\left(-\frac{h\nu_n}{k_B T}\right)} - \sum_n \ln\left(1 - \exp\left(-\frac{h\nu_n}{k_B T}\right)\right) \right] \quad \textbf{(S5)}$$

$$S_{rot}(i,T) = N_A k_B \ln\left[\frac{\sqrt{\pi}}{\sigma} \left(\frac{8\pi^2 k_B T}{h^2}\right)^{\frac{3}{2}} \sqrt{I_{x,i} \times I_{y,i} \times I_{z,i}} \right] \text{ (nonlinear molecules)} \quad \textbf{(S6)}$$

$$S_{rot}(i,T) = N_A k_B \ln\left[\frac{1}{\sigma}\left(\frac{8\pi^2 k_B T}{h^2}\right) I_i\right] \quad \text{(linear molecules)} \tag{S7}$$

$$S_{trans}(i,T,P) = N_A k_B \left(\frac{5}{2}\ln(T) - \ln(P) + \frac{5}{2}\ln(M_i) - 1.165\right) \tag{S8}$$

where the vibrational contributions can be deduced from the calculated frequencies ν_n of the model (note that equation **(S3)** includes the zero point vibrational energy in its first term). $I_{x,i}$, $I_{y,i}$, $I_{z,i}$ (Ii for a linear molecule) are the moments of inertia of the molecule i, and M_i its molecular mass. Rotational contributions have been calculated using the Colby Rotational Constant Calculator (http://www.colby.edu/chemistry/PChem/scripts/ABC.html).[7]

For an adsorbed molecule or for a surface, the rotational and translational contributions are converted into vibration modes, so that the only remaining terms are the vibrational ones – that can be calculated using the equations **(S2)** and **(S5)** – and the electronic energy $E(i)$. For these phases, we also consider that the PV_m term is very small with regard to the energetic terms, and is therefore neglected, and thus we consider $H = U$ in this case.

2. Sample preparation method and characterization

Support. Commercial ZrO_2 (DK-1 from DAIICHI KIGENSO KAGAKU KOGYO CO., LTD., 25 $m^2.g^{-1}$ from BET analysis of N_2 physisorption measurement) was calcined at 500 °C for 2 hours to remove organic impurities. The support was then partially dehydroxylated at 500°C for 20 h under high vacuum (10^{-5} mbar), and then cooled down to room temperature prior storage under argon atmosphere. This sample is referred to as $ZrO_{2\text{-}500}$. The support shows the Powder X-Ray Diffraction (pXRD) pattern of monoclinic zirconia (Figure S1-(a)).
Commercial SiO_2 (AEROSIL 200, Evonik, S_{BET} = 206 $m^2.g^{-1}$) was partially dehydroxylated at 500, for 20 h under high vacuum (10^{-4} mbar), and then cooled down to room temperature prior storage under argon atmosphere. This support is referred to as $SiO_{2\text{-}500}$.

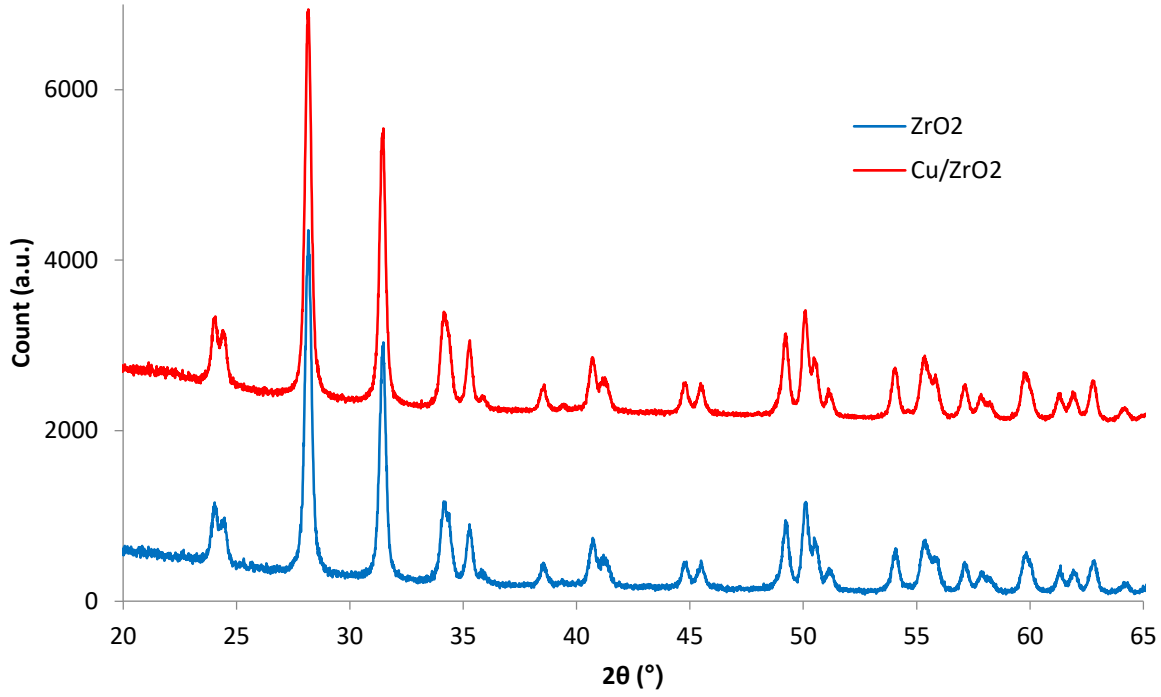

Figure S1. XRD pattern of ZrO_2 (a) before (b) after copper particle synthesis. Only monoclinic zirconia phase is detected (International Center for Diffraction Data, Entry 00-083-0939).

Copper particles synthesis and characterization. All samples were prepared by the grafting method using copper (I) *tert*-butoxide,[8] $[Cu(O^tBu)]_4$, as a precursor. 100 mg of $[Cu(O^tBu)]_4$[9] were dissolved in dry pentane (20 mL). The solution was contacted with 1.0 g of the zirconia support under argon atmosphere in a double Schlenk. After 4 hours of stirring at room temperature, the solid was washed three times with 20 mL of pentane to remove unreacted copper precursor and dried under high vacuum conditions (~10^{-5} mbar). The sample was reduced at 500 °C under H_2 atmosphere for 5 h. After reduction, the sample was cooled down to room temperature under H_2, before vacuum treatment and storage under argon.
The operation can be followed by IR spectroscopy at the various stages of the preparation. Figure S2-(a) shows the IR spectrum of $ZrO_{2\text{-}500}$, that mainly displays ν-OH stretching frequencies at 3774 and 3670 cm^{-1} related to Zr-OH hydroxyl groups. After grafting, C-H stretching bands appear around 2966 cm^{-1} while the intensity of the Zr-OH bands is strongly decreased (Figure S2-(b)). This confirms the grafting of the molecular precursor by chemical reaction with the Zr-OH groups according to Scheme S1. Upon reduction, the ν-CH bands

disappear while the ν-OH bands reappear as an indication that the ligands are decomposed (Figure S2-(c)). At the same time, the color of the sample turns from pale yellow to pink, and particles can be observed by TEM (see below). Scheme S1 shows a schematic representation of the whole process. Finally, the copper content (0.8 %) was determined by ICP (Inductively Coupled Plasma) spectroscopy.

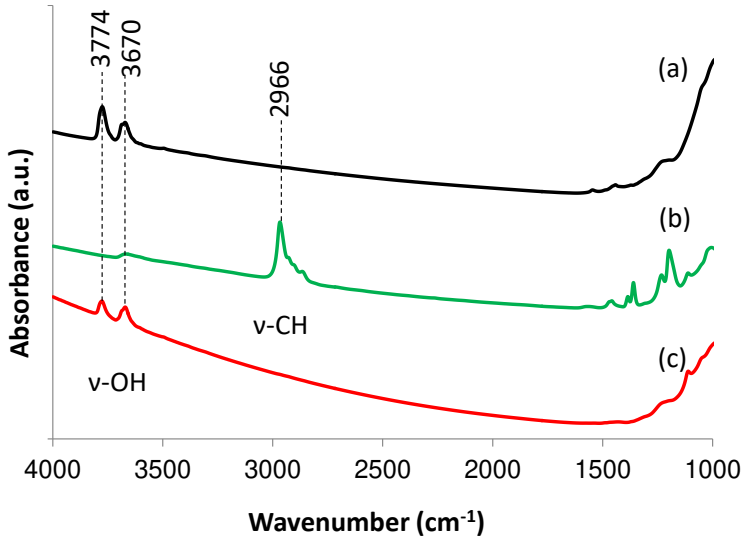

Figure S2. FTIR spectra of the sample during preparation. (a) $ZrO_{2\text{-}500}$ (b) grafted $[Cu(O^tBu)]_4$ on $ZrO_{2\text{-}500}$ (c) after reduction under H_2 at 500 °C for 5 hours.

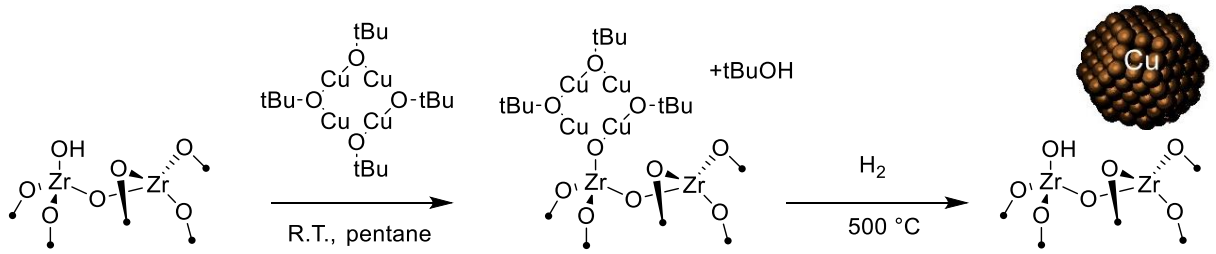

Scheme S1. Schematic representation of the grafting-reduction sequence.

The pXRD pattern remains unchanged by this procedure (Figure S1-(b)). No diffraction peak for copper could be detected. TEM imaging shows indeed that the copper particles are small (2.2 ± 0.5 nm) and thus below the detection limit of pXRD (Figure S3-(a)).
A $Cu/SiO_{2\text{-}500}$ sample was prepared according to a similar synthesis method. Using 100 mg of $[Cu(O^tBu)_4]$ in pentane for 1 g of silica yields a sample with 3.7 % of copper loading after grafting and reduction (H_2, 500 °C, 5 hours). TEM imaging on Figure S3-(b) shows the particles and the particle size distribution for this catalyst.

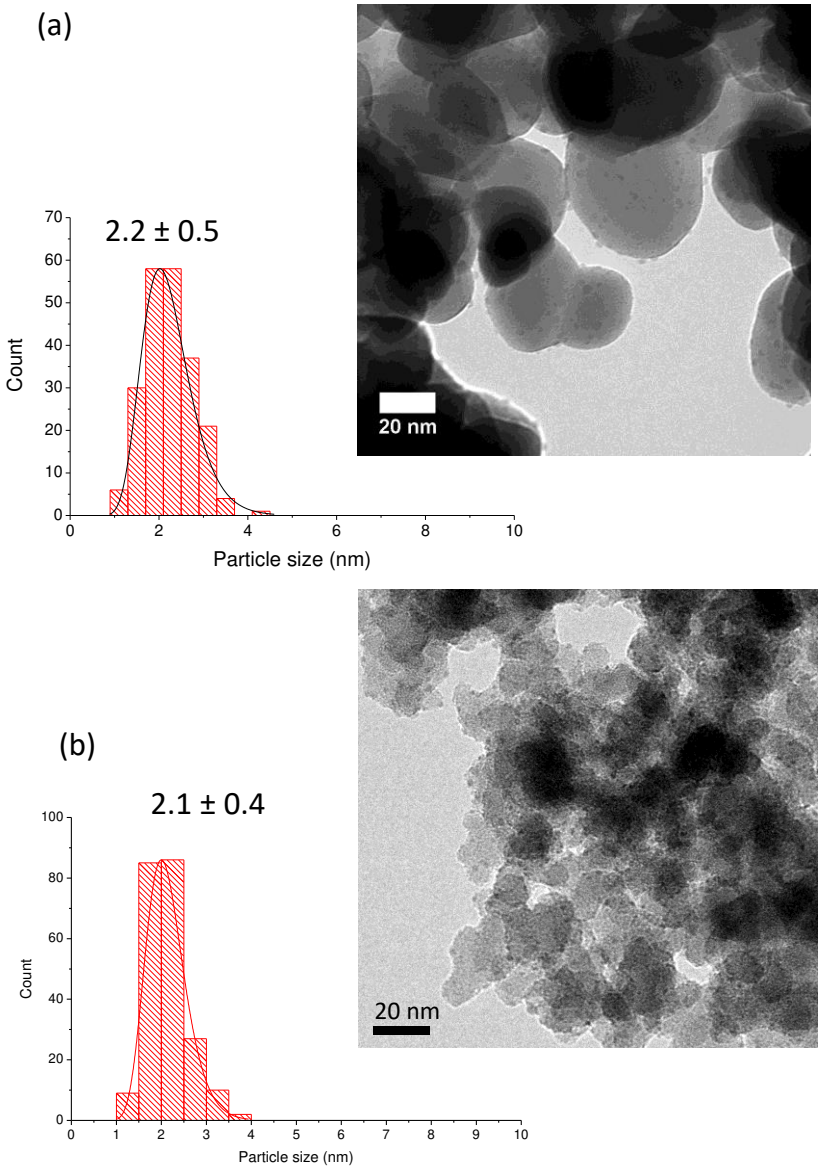

Figure S3. (a) TEM imaging and particle size distribution of $Cu/ZrO_{2\text{-}500}$ prepared as described above (b) TEM imaging and particle size distribution of $Cu/SiO_{2\text{-}500}$ prepared as described above

3. Catalytic testing in flow reactor

The CO_2 hydrogenation was conducted in a fixed-bed tubular reactor at 25 bars (PID Eng&Tech). The reaction temperature was measured at the catalyst bed by a K-type thermocouple. After loading about 300 mg of a catalyst powder and 5.0 g of SiC in the reactor under air, the catalyst was treated under a flow of 17%H_2/N_2 (60 mL min^{-1}) at 300 ºC for 30 min under ambient pressure. After cooling to 270 ºC, a flow of CO_2/H_2/N_2 (1/3/1, 62 mL min^{-1}) was passed through the catalyst bed for 12 h at 25 bar. The conditions were then set to the measurements conditions (230 °C, 25 bars), and the products were analyzed by an online gas chromatograph (Agilent 7890A) equipped with FID (for methanol) and TCD (N_2, CO_2, CO, CH_4). In all experiments, CH_4 concentration in the outlet gas was negligible.
The formation rates of CO and MeOH and the selectivity to methanol were calculated using the following equations.

$$F_{out}\,[\mathrm{mol\,h^{-1}}] = \frac{F_{in} \times C_{N_2,in}}{C_{N_2,out}} \quad \textbf{(S9)}$$

$$r_x\,[\mathrm{mol_x\,h^{-1}\,g_{Cu}^{-1}}] = \frac{F_{out} \times C_{x,out}}{w_{Cu}} \quad \textbf{(S10)}$$

$$S_{MeOH} = \frac{F_{meOH,out}}{F_{CO,out}+F_{MeOH,out}} \quad \textbf{(S11)}$$

where F_{in} is a total gas inlet flow rate (mol h^{-1}), F_{out} is a total gas outlet flow rate (mol h^{-1}), $C_{x,in}$ is the inlet gas fraction of species x, $C_{x,out}$ is the outlet gas fraction of species x, r_x is the production rate of species x (mol_x h^{-1} g_{cat}^{-1}) and w_{Cu} the copper content in the catalytic bed (g_{Cu}). The volumetric flow rate Q (in mL.min^{-1}) of the feed was decreased in order to increase the contact time (defined as m_{cat}/Q). Each flow rate was kept constant for about 4 hours before switching to the next one. For each flow rate, the formation rates of CO and methanol are constant save for a rather large scatter of the CO rate due to the integration of from rather small TCD peaks (Figure S4 (a) and (b)). After about 30 hours on stream, the flow rate is changed back to the initial value. On Cu/SiO_2 the initial value is recovered, indicating negligible deactivation. On Cu/ZrO_2, slightly lower values are obtained (about 10 % lower than the initial one), indicating a very slow deactivation process for both CO and methanol productions. Thus, steady-state is a good approximation for both catalysts. The five points were averaged for the calculation of the formation rates and selectivities for a given contact time (flow rate). The rates were extrapolated using a second order polynomial function. This function has no physical meaning and is merely used to allow for estimating the initial rates at zero conversion – and hence selectivities.

(a) Cu/ZrO_2

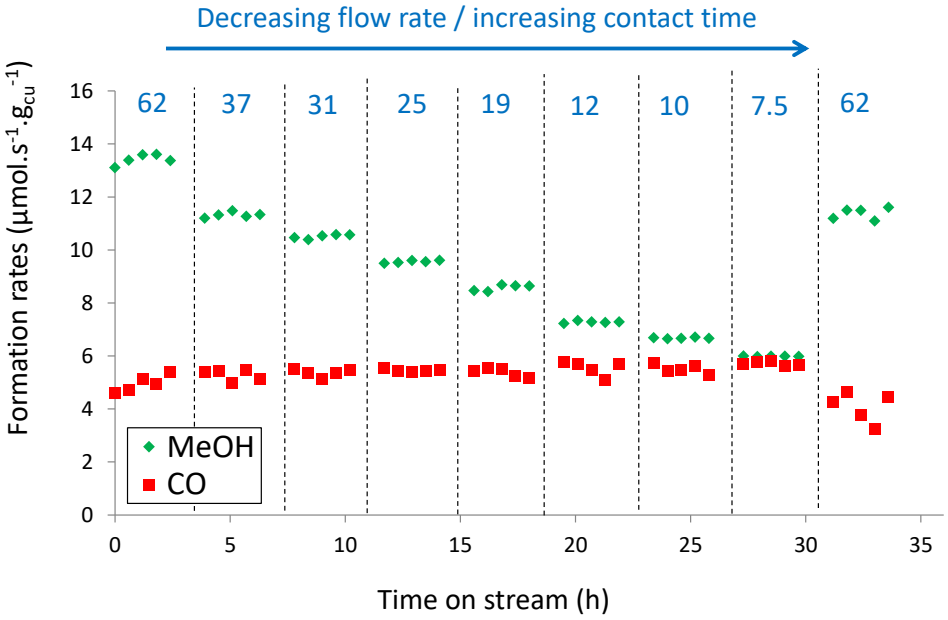

(b) Cu/SiO_2

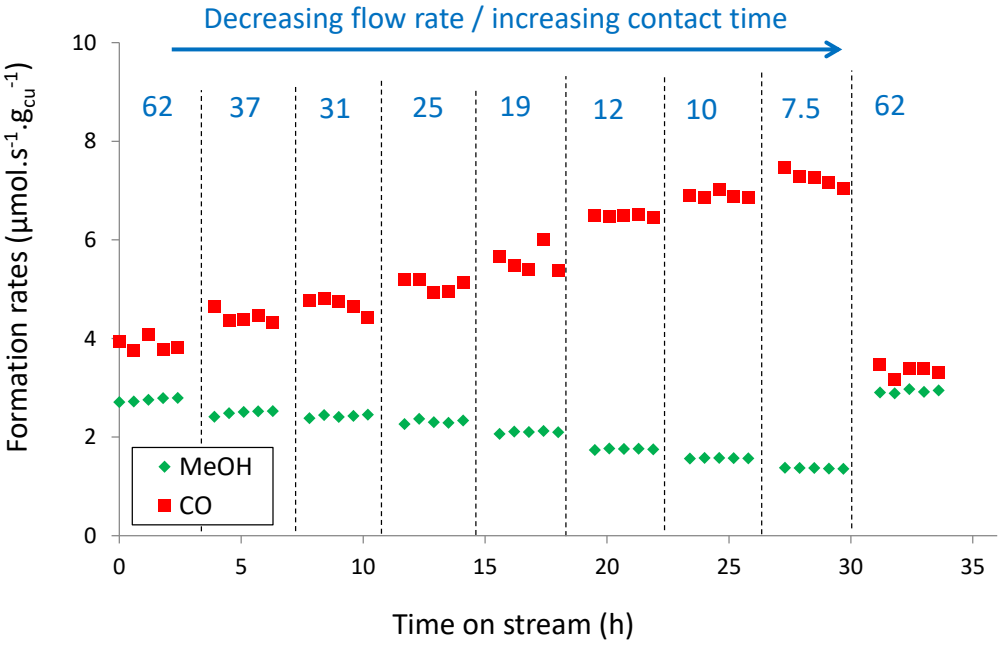

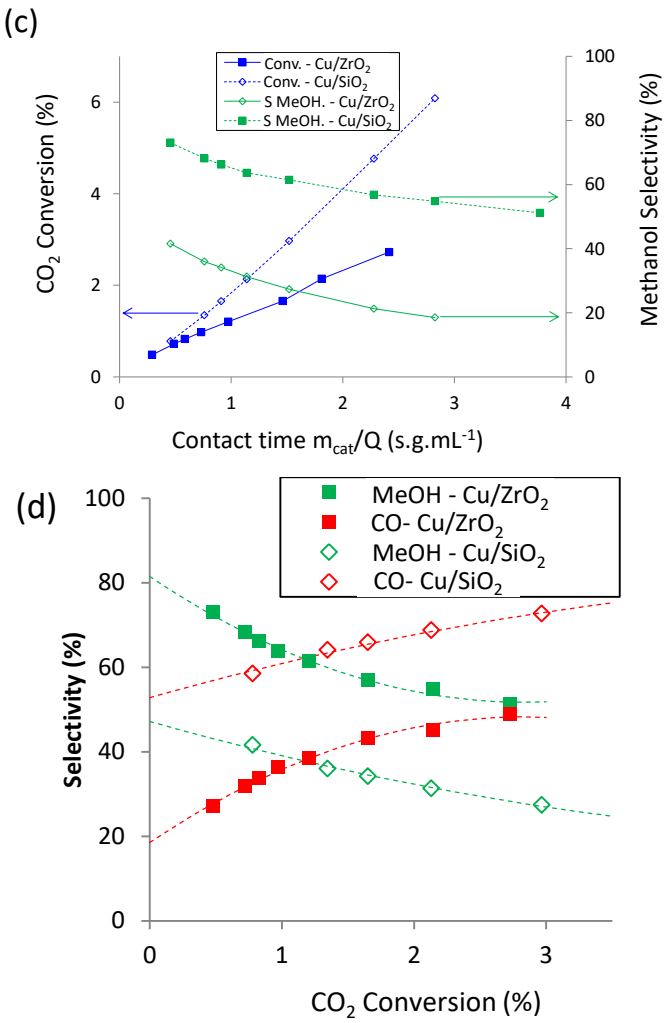

Figure S4. Catalytic results of the hydrogenation of CO_2 in a flow reactor (230 °C, 25 bars of $H_2/CO_2/N_2$ (3:1:1), m_{cat} ~ 300 mg) (a) Evolution of the formation rates with time on stream for Cu/ZrO_2 (b) Evolution of the formation rates with time on stream for Cu/SiO_2(c) Evolution of the CO_2 conversion and methanol selectivity with contact time. (d) Selectivity versus conversion plot.

4. Additional IR spectroscopic measurements

Ex-situ IR measurements. Similarly to the *Ex-Situ* NMR spectra presented in the main article (Figure 1), *Ex-situ* IR measurements were recorded after reaction of Cu/ZrO_2 in a closed vessel with $^{13}CO_2$ and H_2 and/or D_2, followed by evacuation of the gas-phase under high vacuum (10^{-4} mbar).

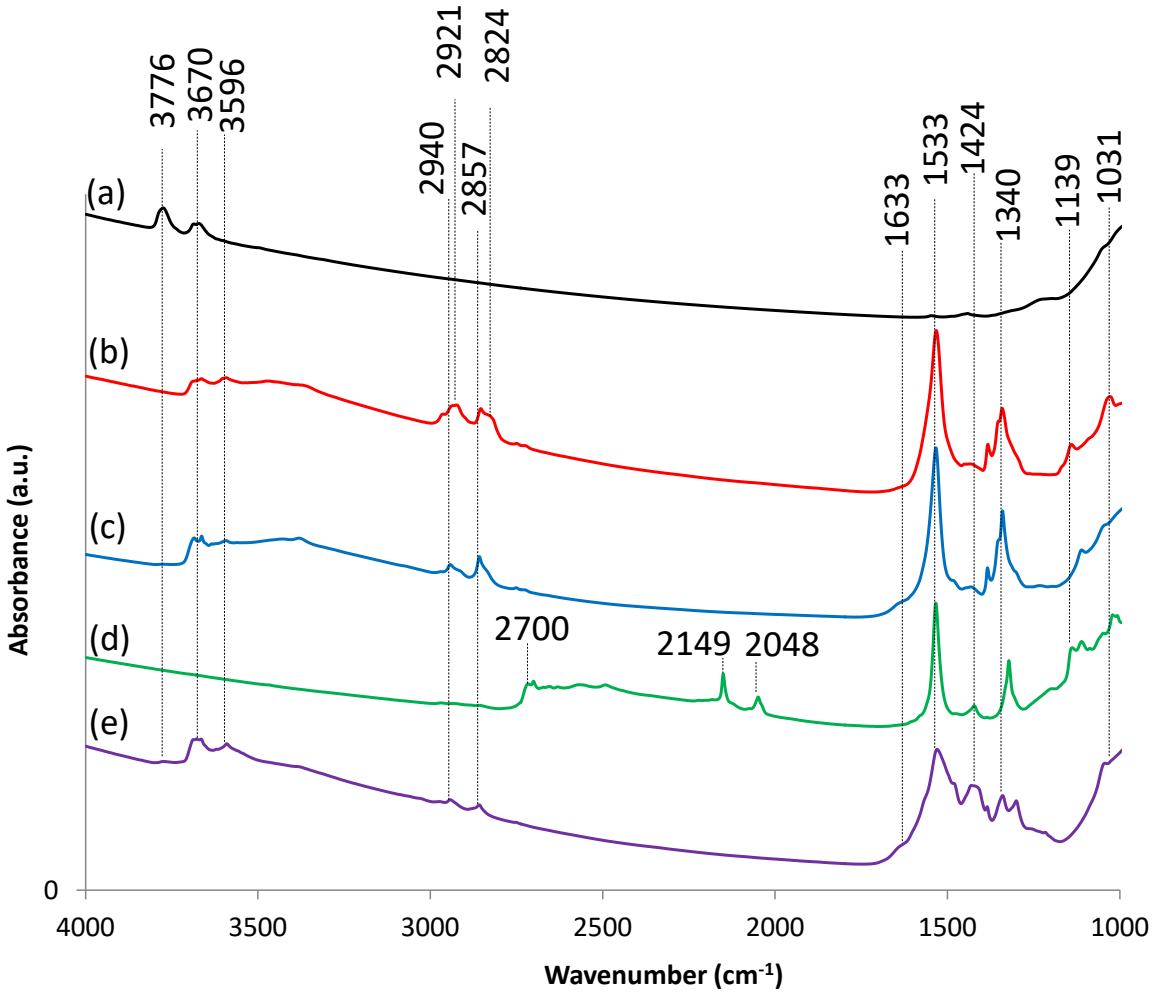

Figure S5. (a) IR spectra of the starting Cu/ZrO_2 sample. **(b-e)** *Ex-situ* IR spectra taken after reaction of Cu/ZrO_2 with $^{13}CO_2$ and H_2 at 230 °C for 12 hours at **(b)** 5 bars **(c)** 1 bar **(d)** After reacting sample from spectrum (b) with D_2 (5 bars) at 230 °C for 12 hours **(e)** *Ex-situ* IR spectrum taken after reaction of pure ZrO_2 with $^{13}CO_2$ and H_2 at 230 °C for 12 hours at 5bars.

In situ DRIFTS measurements.

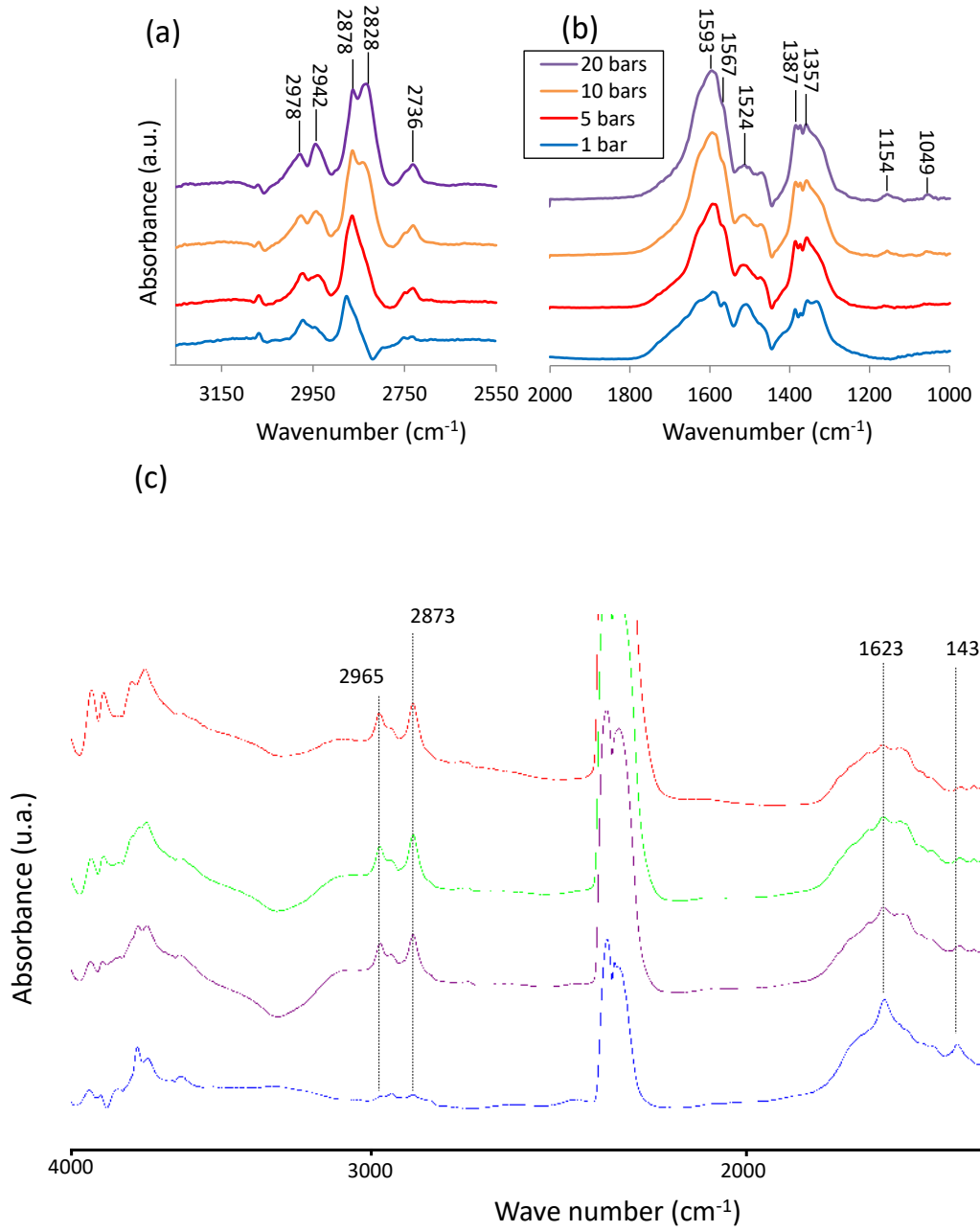

Figure S6. *In situ* DRIFT spectra of Cu/ZrO_2 at 230 °C under 1 to 20 bars of a H_2/CO_2 mixture in the regions of the **(a)** C-H stretching and **(b)** C-O stretching frequencies. The DRIFT spectra recorded under H_2 flow at the reaction temperature were used as the background. **(c)** *In situ* DRIFT spectra of pure ZrO_2 contacted with a CO_2/H_2 mixture (1:3) at 230 °C and at various pressures (1 to 20 bars).

5. Adsorption of Formic acid and methanol on the catalysts (Cu/SiO_2 and Cu/ZrO_2)

In order to assign the spectroscopic signals observed during reaction, we adsorbed formic acid on the catalysts and measured IR spectra and ^1H solid-state NMR spectra. A small amount of the reduced sample is loaded in a glass tube in an Ar glovebox. The tube is evacuated at room temperature under high vacuum (10^{-4} mbar), and the solid is contacted with either 30 mbar of formic acid or 80 mbar of methanol for 5 minutes. The gas-phase is then evacuated under high vacuum at room temperature for 6 hours. The sample is then transferred back in a glovebox, where the IR spectrum is recorded. In the case of formic acid, the sample is packed into a 2.5 mm rotor and a MAS NMR ^1H spectrum is recorded (spinning rate 20 kHz).

Detection of formate adsorbed on copper by NMR

The adsorption of formic acid on silica gives rise to small features at 2946 cm^{-1} and 1734 cm^{-1} (Figure S7). The latter band is similar to the C=O stretching frequency of gas-phase formic acid. Thus these features can be assigned to formic acid bound to silica through hydrogen bonding. The ^1H NMR spectrum shows a weak signal at 8.7 and 8.4 ppm. The region between 0 and 5 ppm shows several peaks that are already present in the silica itself, thus the changes can be attributed to perturbation of the hydrogen bond network (Figure S8).

Adsorption of formic acid on Cu/SiO_2 shows the band at 1735 cm^{-1} and two additional features in the C=O region at 1668 and 1549 cm^{-1}, that are consistent with formic acid adsorbed on copper and formate on copper, respectively (see Table S2). These are associated to bands in the CH region at 2858, 2876, 2938 and 2954 cm^{-1}. These bands are much stronger in intensity than the CH band of formic acid on silica, suggesting a much greater surface species concentration (Figure S7). Thus, in this sample, three species coexist: formic acid on silica, formic acid on copper and formate on copper. However, the MAS NMR ^1H spectrum shows no additional signal around 5-10 ppm (Figure S8).

On the contrary, formic acid adsorbed on ZrO_2 or Cu/ZrO_2 shows strong IR frequencies in the CH region at 2962, 2932, 2875, 2854 cm^{-1} and 1565 and 1387 cm^{-1} in the CO region (Figure S9), that are attributed to formate adsorbed on zirconia. Very little difference is observed between Cu/ZrO_2 and ZrO_2, suggesting that most species are on the support. MAS NMR ^1H spectrum (Figure S10) also shows a strong signal at 8.8 ppm.

Adsorption of formic acid on Cu/SiO₂ and SiO₂

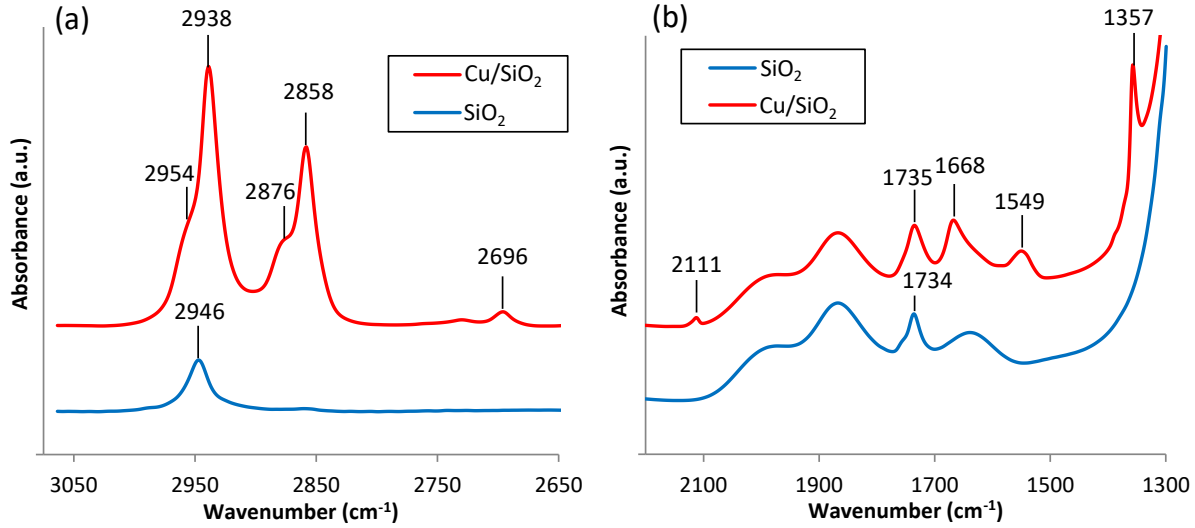

Figure S7. FTIR spectra of formic acid adsorbed on Cu/SiO_2 and SiO_2, after evacuation at room temperature overnight. Spectra are normalized with respect to the Si-O-Si bands of silica between 2100 and 1500 cm^{-1}.

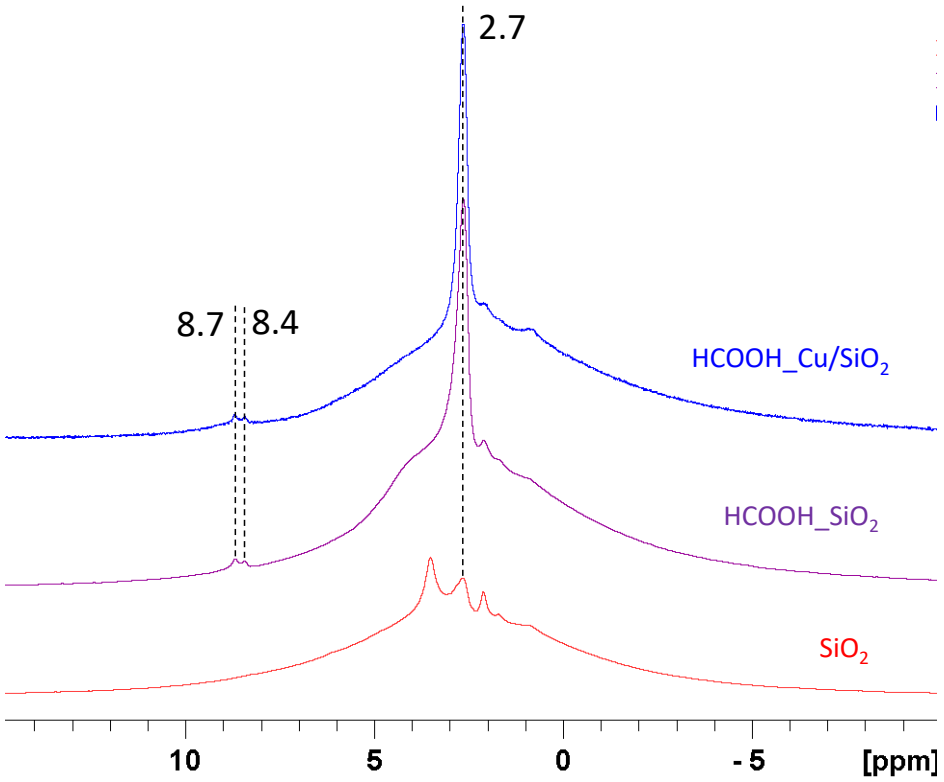

Figure S8. Solid-state MAS NMR ^1H NMR of formic acid adsorbed on SiO_2 or Cu/SiO_2. The starting silica is also shown. Spectrometer 700 MHz (16.5 T), MAS frequency 20 kHz, 200 scans, line broadening 50 Hz.

Adsorption of formic acid on Cu/ZrO₂ and ZrO₂

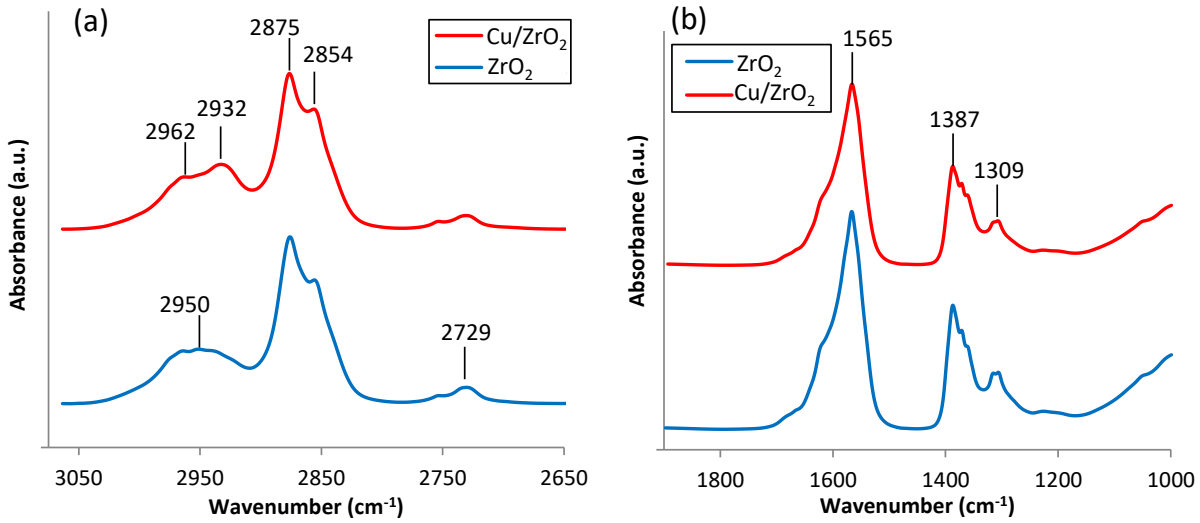

Figure S9. FTIR spectra of formic acid adsorbed on Cu/ZrO_2 and ZrO_2 after evacuation at room temperature overnight.

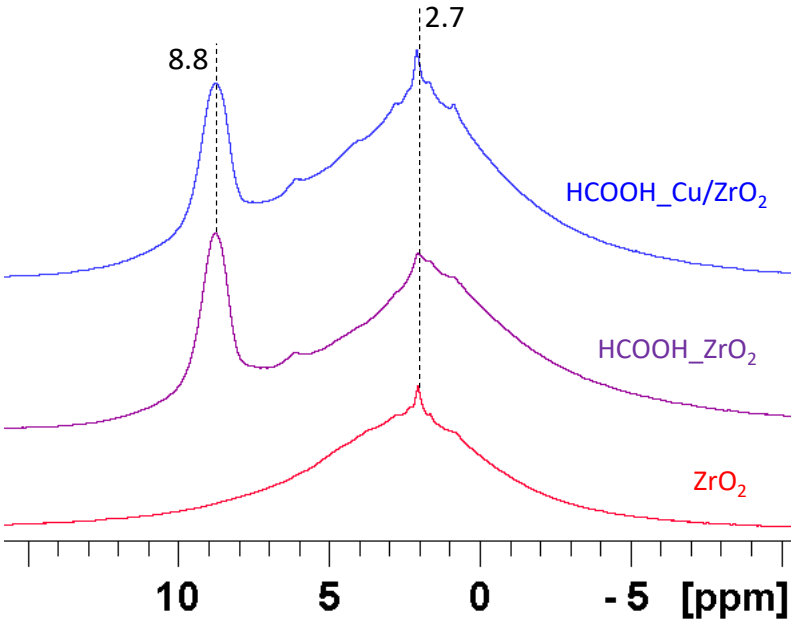

Figure S10. Solid-state MAS NMR ^{1}H NMR of formic acid adsorbed on ZrO_2 or Cu/ZrO_2. The starting zirconia is also shown. Spectrometer 700 MHz (16.5 T), MAS frequency 20 kHz, 200 scans, line broadening 50 Hz.

Adsorption of methanol on Cu/SiO₂ and SiO₂

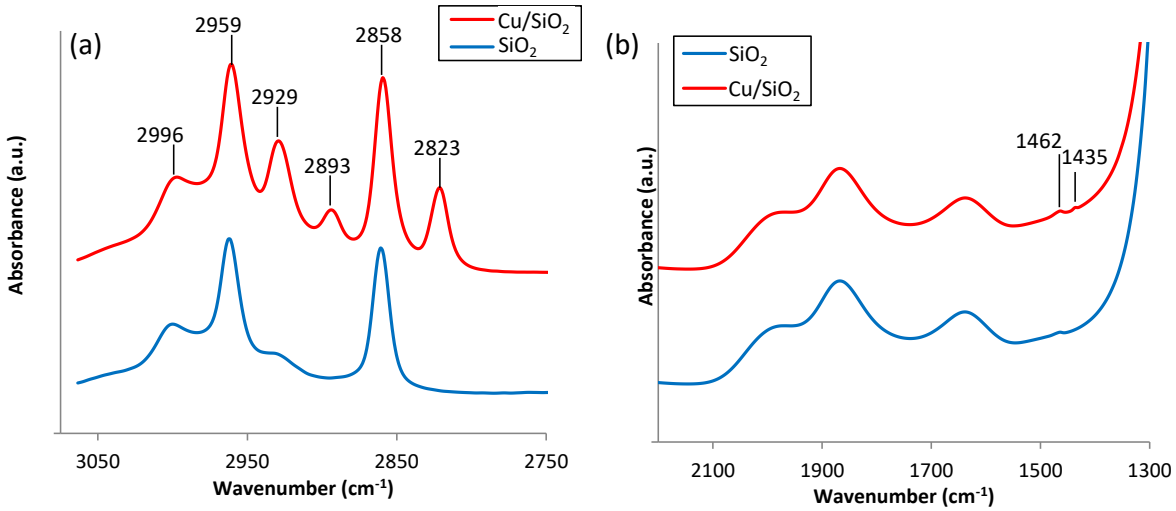

Figure S11. FTIR spectra of methanol adsorbed on Cu/SiO_2 and SiO_2. Spectra are normalized with respect to the Si-O-Si bands between 2100 and 1500 cm^{-1}.

Adsorption of methanol on Cu/ZrO₂ and ZrO₂

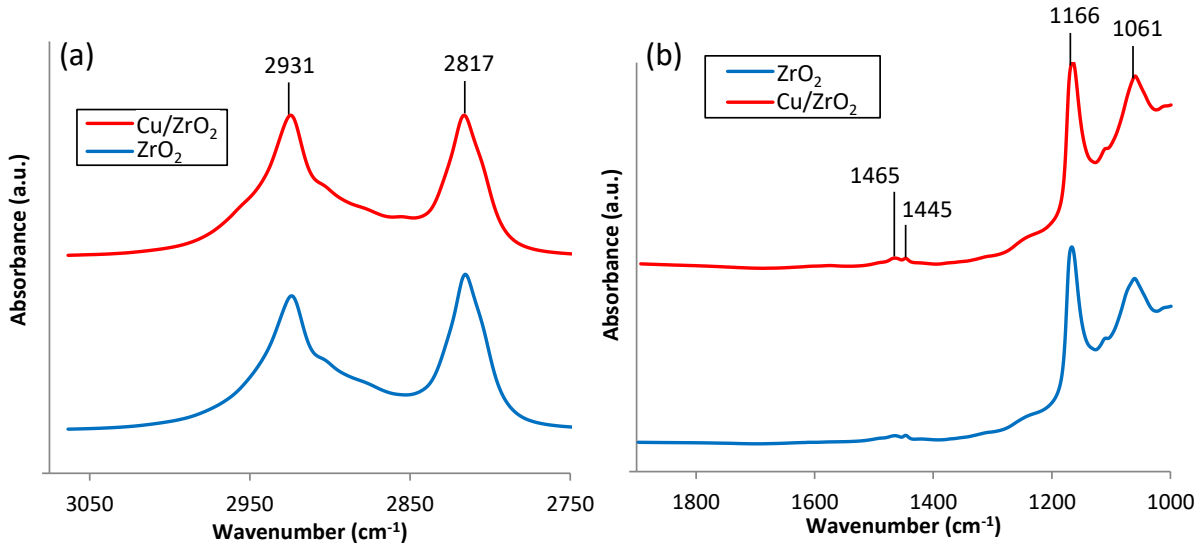

Figure S12. FTIR spectra of methanol adsorbed on Cu/ZrO_2 and ZrO_2.

6. Reaction of CO_2 and H_2 on Cu/SiO_2

The $^{13}CO_2$ hydrogenation at 5 bars and 230 °C in batch as reported for Cu/ZrO_2 was also performed on the Cu/SiO_2 sample according to a similar procedure. Solid-state ^{1}H and ^{1}H-^{13}C CP-MAS NMR spectra were recorded. Figure S13 compare the spectra obtained with Cu/ZrO_2 and Cu/SiO_2. On the proton NMR spectrum, Cu/ZrO_2 shows quite intense signals at 8.4 and 4.1 ppm for formate and methoxy, respectively. With Cu/SiO_2, no signal is observed in the 7-10 ppm region, although more scans were used to record this one (256 vs. 64 on Cu/ZrO_2). On the CP-MAS ^{13}C spectrum, intense signals are obtained on Cu/ZrO_2 at 166 and 52 ppm while we could only observe a very weak and broad signal at 168 ppm (formate) with Cu/SiO_2. In the latter case, longer mixing times (2 ms vs. 0.5 ms) and much more scans (7344 vs. 64) where

used, which should have resulted in stronger signals. This signal can be assigned to formate adsorbed on copper, as confirmed by IR spectroscopy (see Figure S13, performed with $^{12}CO_2$ and H_2 to allow comparison with spectra in Figures S7 to S12),[10] although its observation by NMR is made very difficult because of fast relaxation of the polarization. Alternatively, it might arise from very small amounts of formate or formic acid spilt over to silica.

To confirm the presence of formate only at the surface of Cu/SiO_2, the catalyst was washed with D_2O after the reaction (without exposure to air), and liquid ^{13}C NMR of the supernatant was measured (Figure S15). The signal at 168 ppm of formic acid appears, while no methanol is observed.

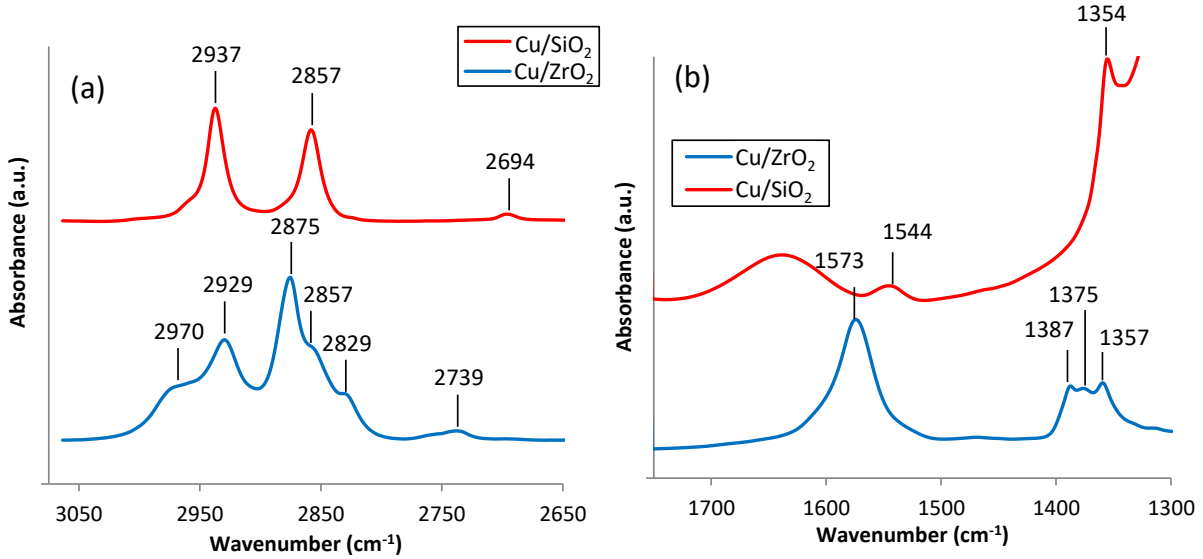

Figure S13. FTIR spectra of $^{12}CO_2$ and H_2 reacted at 5 bars and 230 °C for 12 hours on (a) Cu/ZrO_2 (b) Cu/SiO_2.

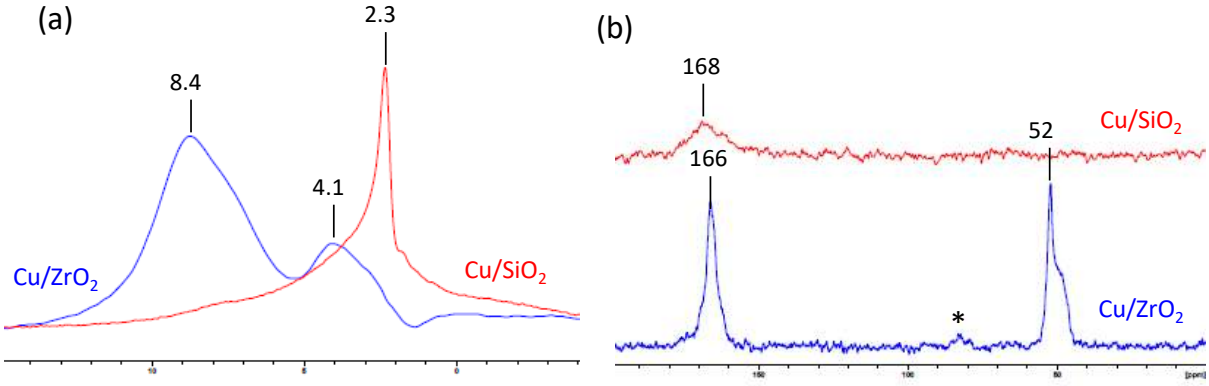

Figure S14. (a) Ex-situ MAS NMR ^1H spectrum of $^{13}CO_2$ and H_2 reacted with Cu/SiO_2 (NS = 256) or Cu/ZrO_2 (NS = 64) at 5 bars and 230 °C for 12 hours (b) Ex-situ CP-MAS NMR ^{13}C-^1H spectrum of $^{13}CO_2$ and H_2 reacted with Cu/SiO_2 (NS = 7344, mixing time 2 ms) or Cu/ZrO_2 (NS = 64, mixing time 0.5 ms) at 5 bars and 230 °C for 12 hours. No HETCOR spectrum could be recorded on Cu/SiO_2. * : spinning side band.

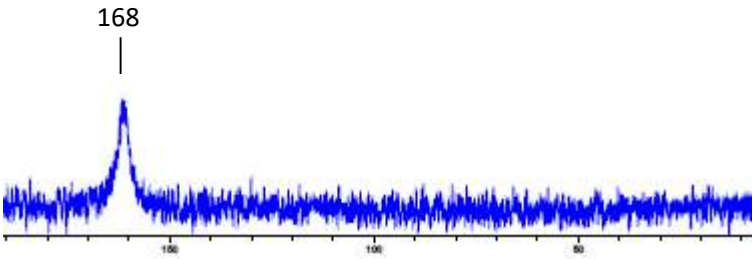

Figure S15. Liquid ^{13}C NMR spectrum of the supernatant of Cu/SiO_2 washed with D_2O.

7. Additional solid-state NMR spectra

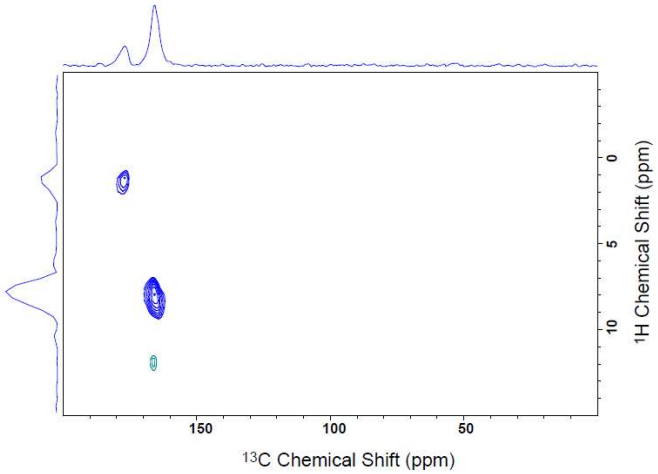

Figure S16. Ex-situ MAS NMR ^{1}H-^{13}C HETCOR spectrum of ZrO_2 after reaction with $^{13}CO_2/H_2$ (1:3) at 5 bar and 230 °C. The signal at $\delta(^{13}C) = 167$ ppm, $\delta(^{1}H) = 8.0$ ppm is attributed to formate, the signal at $\delta(^{13}C) = 179$ ppm, $\delta(^{1}H) = 1.6$ ppm to bicarbonate.

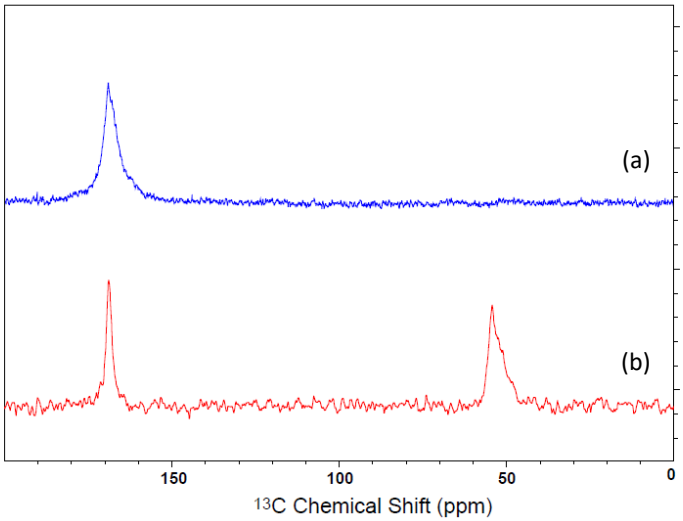

Figure S17. Ex-situ MAS NMR ^{13}C direct excitation spectra of Cu/ZrO_2 (a) after contacting $^{13}CO_2/H_2$ (1:3) at 1 bar at 230 °C (b) after contacting the sample from spectrum (a) with 5 bars of D_2. The recycle delay of spectrum (b) was set as 240 s in order to have a quantitative analysis. Neither carbonate (expected at 180-210 ppm) nor CO_2 (around 120 ppm) can be observed.

8. Liquid state NMR spectroscopy

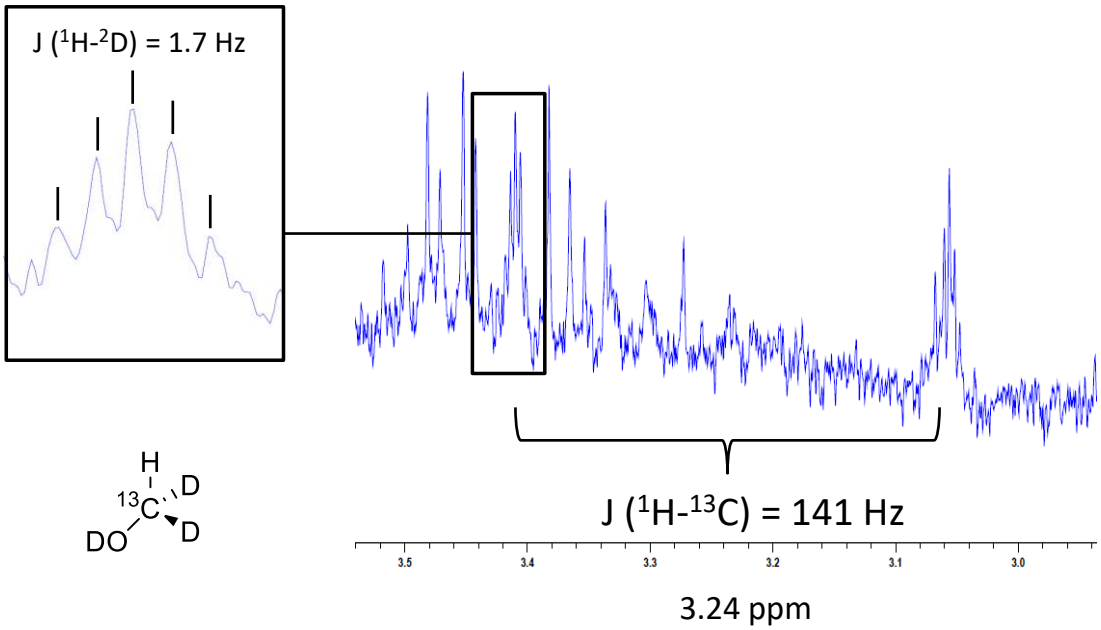

Figure S18. Liquid-state ^{1}H NMR after washing Cu/ZrO_2 with D_2O after the two steps hydrogenation of $^{13}CO_2$. A doublet of pentet centered at 3.24 ppm can be observed, related to the ^{1}H-^{13}C and ^{1}H-^{2}D J-couplings. This is consistent with a $^{13}CHD_2$ group. This signal merges into a single peak at 3.24 ppm when a ^{13}C decoupling pulse is applied. The other peaks are impurities introduced during the process. They do not change upon ^{13}C decoupling.

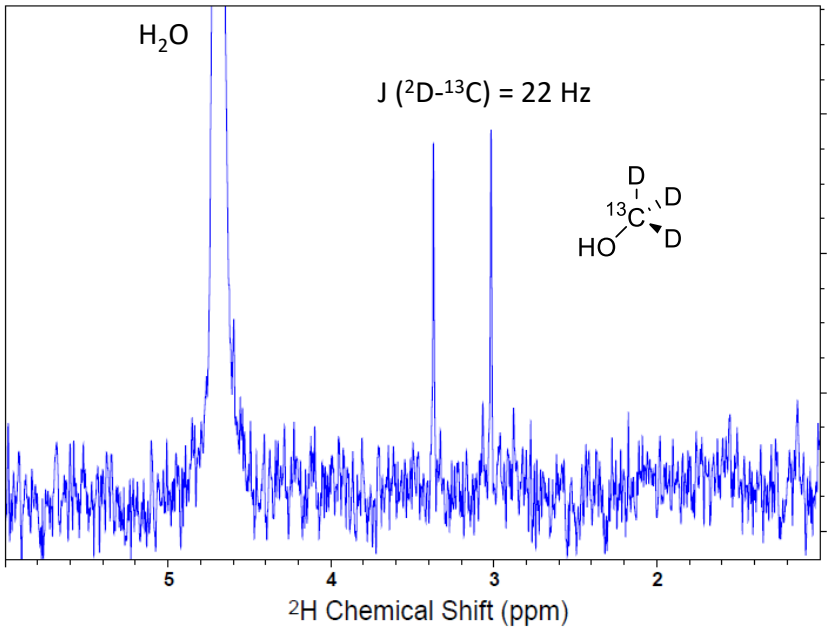

Figure S19. Liquid-state ^{2}D NMR after washing Cu/ZrO_2 with H_2O after the two steps hydrogenation of $^{13}CO_2$. A doublet centered at 3.19 ppm can be observed, related to the ^{2}D-^{13}C J-coupling. No fine structure can be distinguished (no ^{1}H decoupling was applied).

Quantification of the number of desorbed methanol

Based on the deuterium spectrum shown in Figure S19, it is possible to evaluate the number of methanol released in solution, and hence to give a rough estimate of the number of active sites on the catalyst.

The deuterium signal associated to water at 4.7 ppm is due to the naturally abundant deuterium, (0.0115 %). The concentration of proton in water is of 111.1 $mol.L^{-1}$; hence the concentration of deuterium is of 1.3 10^{-2} $mol.L^{-1}$. The peaks assigned to methoxy integrate for 0.041 of the water peak at 4.7 ppm.

If we assume that the predominant form of methanol in solution is CD_3OD, and if we neglect the desorption of some OD groups on the surface in the form of water in solution, we can calculate the concentration of methanol in solution to be 1.8 10^{-4} $mol.L^{-1}$. As 2.0 mL of water were employed to wash the solid, this represents 3.5 10^{-7} mol of methanol.

The spectrum was obtained after washing 200 mg of sample (SSA = 25 $m^2.g^{-1}$). Thus, the surface concentration of adsorbed methanol was of 0.07 $\mu mol.m^{-2}$ (0.04 $methanol.nm^{-2}$). Assuming that one molecule of methanol was adsorbed on each active site, this number should be the number of active sites.

We may also estimate the number of particles at the surface of the catalyst. Considering the loading (0.8 % Cu), the size of the particles (~ 2 nm, which is constituted of about 300 Cu atoms) and the specific surface area, we calculate the average density of particles at the surface to be of 0.01 $particle.nm^{-2}$. This number is about the same order of magnitude than the number of active sites estimated (~ 4 sites/particles), which rather supports the involvement of a small number of interfacial sites – although these estimates are quite rough.

9. Additional DFT structures

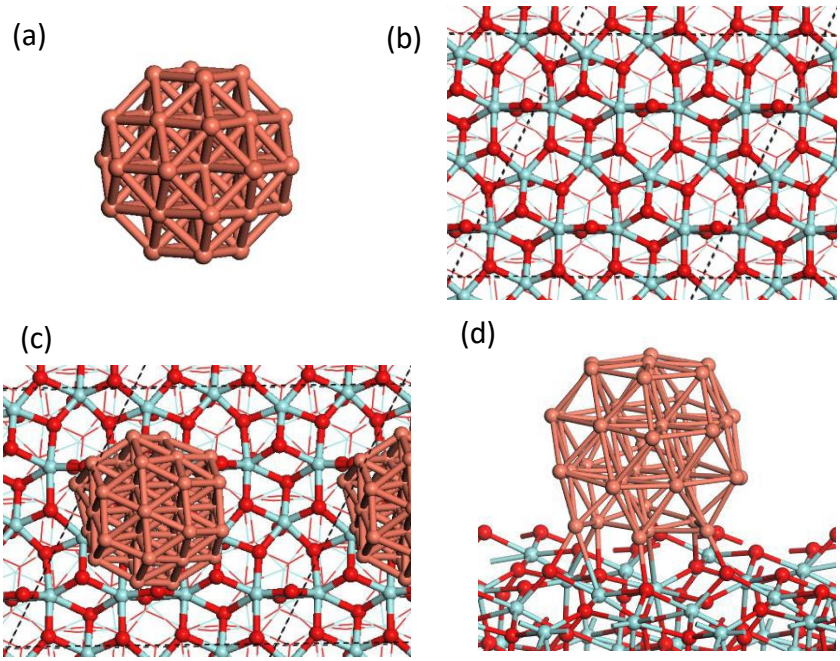

Figure S20. Models for the supported copper particle **(a)** Cu_{38} particle (ø = 0.8 nm) **(b)** moniclinic ZrO_2 slab (top view). The frame highlights the limits of the simulation box. **(c-d)** Optimized Cu_{38}/ZrO_2 model (c) Top view (d) Side view.

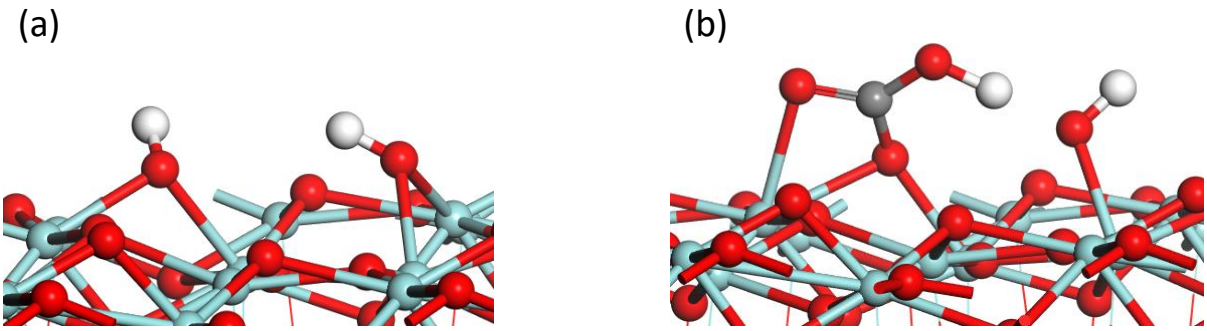

Figure S21. (a) Water molecule adsorbed on the ZrO_2 surface. The molecule is dissociated in two hydroxyl group. (b) Bicarbonate (CO_3H^*) generated by adsorption of CO_2 on one hydroxyl group.

10. Various calculations

Table S1. Calculated ^{1}H and ^{13}C chemical shifts and Bader charges on the carbon atom for various intermediates optimized on the Cu (111) and ZrO_2 ($\bar{1}11$) facets, as well as at interfacial sites of the Cu/ZrO_2 model. When two types of H atoms are present in the intermediate, both are given in the order of the formula.

Surface	Species	δ (^{1}H)	δ (^{13}C)	Charge on C
Cu (111)	COOH*	3.0	219	1.2
	HCOO*	2.6	179	1.6
	HCOOH*	1.0/-1.3	180	1.5
	H_2COO*	1.1	90	0.9
	H_3CO*	-2.6	54	0.4
	H_3COH	-4.1/-4.0	61	0.3
ZrO_2 ($\bar{1}11$)	CO_3*	-	158	2.1
	CO_3H*	15.3	169	2.2
	HCOO*	6.6	180	1.5
	H_2COO*	8.7	87	1.1
	H_3CO*	3.4	67	0.3
Cu/ZrO_2	CO_2*	-	219	1.2
	COOH*	10.9	227	1.1
	HCOO*	6.5	177	1.5
	H_2COO*	9.2	114	1.0
	H_3CO*	3.6	66	0.5
	H_3COH*	3.3	58	0.3
-	$CO_{2(g)}$	-	135	2.1
$CO_{2(g)}$ - experimental		-	125	-

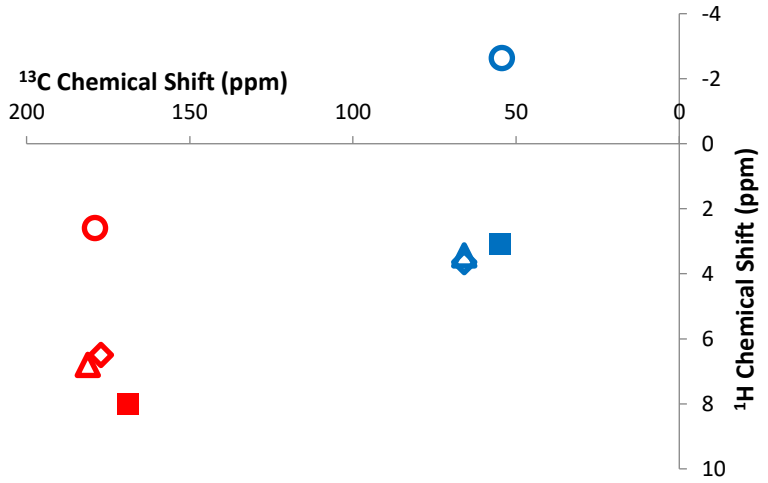

Figure S22. Simulated ^{1}H-^{13}C HETCOR spectra of the formate (red) and methoxy intermediates (blue) on the Cu (111) surface (open circles), on the ZrO_2 ($\bar{1}11$) facet (open diamond) and on the Cu/ZrO_2 interface (open triangles). Experimental points are shown (squares).

Surface	Species	ν_{C-H}	δ_{C-H}	δ_{O-C-H}	ν_{C-O}
Cu (111)	H_3CO*	3028, 3024, 2966	1446,1441,1417	1135,1132	1012
	H_3COH	3078,3023,2949	1455,1440,1421	1135,1046	983
ZrO_2 ($\bar{1}11$)	H_3CO*	2995,2964,2904	1452,1447,1424	1146,1138	1102
Cu/ZrO_2	H_3CO*	2959,2859,2837	1436,1422,1407	1158,1133	1130
	H_3COH*	3093, 3037,2965	1468,1446,1422	1144,1093	1000
$MeOH_{(g)}$		3061, 2980,2944	1461,1449,1433	1130,1062	1010

Table S2. Calculated vibration frequencies for the formate/formic acid and methanol/methoxy intermediates

Surface	Species	ν_{C-H}	ν_{O-C-O}	δ_{C-H}	δ_{C-O}
Cu (111)	HCOO*	2954	1529	1318, 1313	983
	HCOOH*	3001	1663	1360,1289	1001
ZrO_2 ($\bar{1}$11)	HCOO*	2980	1532	1348,1365	1014
	HCOOH*	2895	1694	1340,1202	1002
Cu/ZrO_2	HCOO*	3014	1525	1369,1330	1056
$HCOOH_{(g)}$		2984	1763	1352,1261	1000

11. Methanol synthesis on the Cu(111) surface

There are some mechanistic differences during CO_2 hydrogenation to methanol. The hydrogenation on Cu(111) surface via a formate (HCO_{2*}) intermediate shows that in contrast to Cu/ZrO_2, the reduction of formate (HCO_{2*}) to acetal (H_2CO_{2*}) is less favorable than going through formic acid (HCO_2H*) with a difference in overall activation barrier of $\Delta\Delta G^{\ddagger}$ = 20 kJ/mol. The overall activation barrier for the favored pathway is $\Delta G^{\ddagger}$ = 267 kJ/mol. The difference in preferred reaction mechanism is due to the Lewis acidic site of ZrO_2 which can bind more strongly the reaction intermediates and hence favors to hydrogenate carbon a second time to keep the bidentate bonding. The decomposition of hydroxymethoxy (H_2CO_2H*) to methoxy (CH_3O*) and hydroxyl ($OH*$) happens in a stepwise fashion by first forming formaldehyde and hydroxide upon which the formaldehyde gets further reduced to methoxy (CH_3O*).

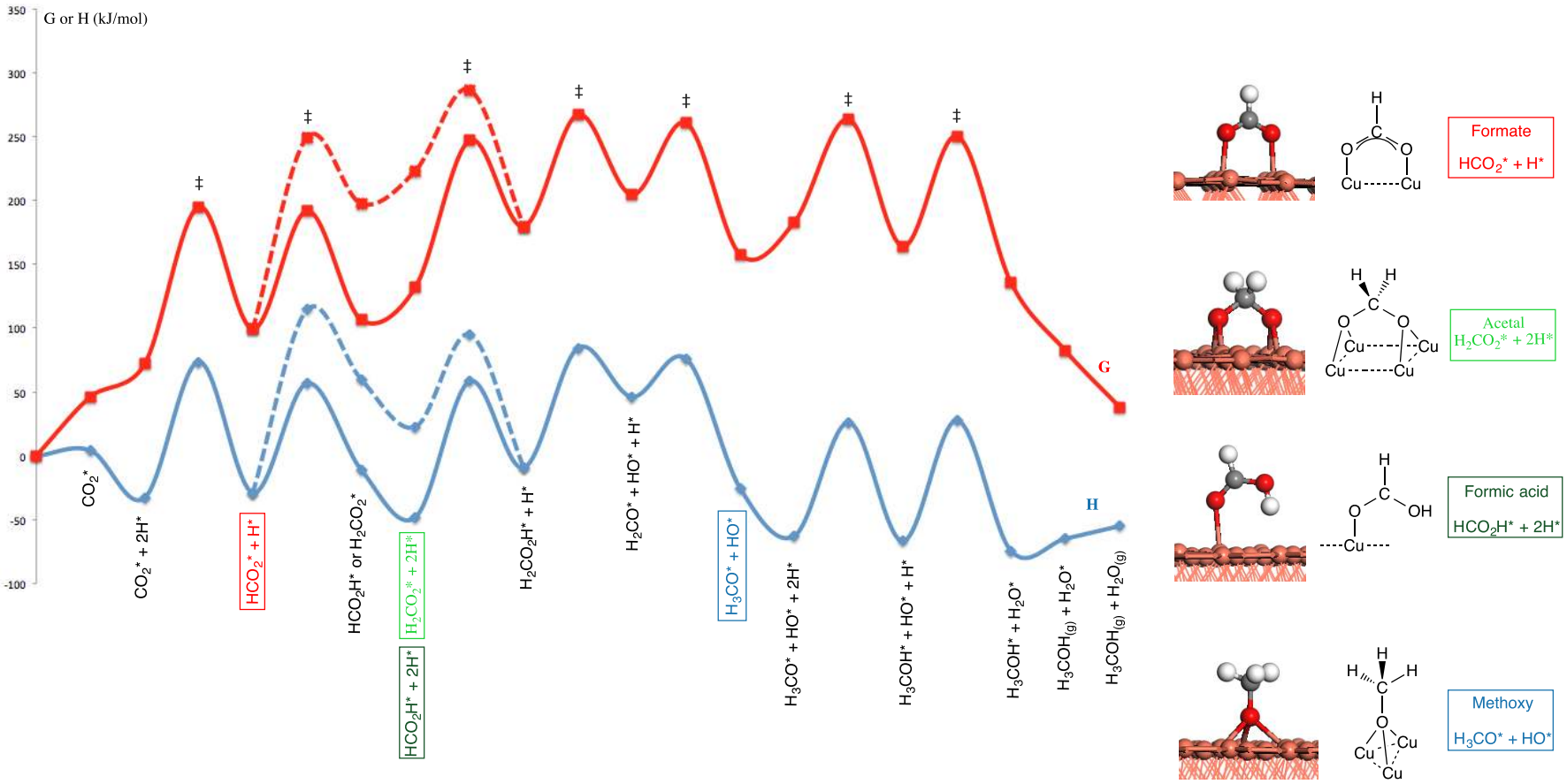

Figure S23. Enthalpy and Gibbs free energy at 475 K for the hydrogenation of CO_2 to methanol on Cu(111) surface via two mechanistic pathway via formic acid (straight line) and acetal (dashed line).

REFERENCES

[1] A. Urakawa, N. Maeda, A. Baiker, *Angew. Chem. Int. Ed.* **2008**, *47*, 9256-9259.

[2] A. Lesage, D. Sakellariou, S. Hediger, B. Elena, P. Charmont, S. Steuernagel, L. Emsley, *J. Magn. Reson.* **2003**, *163*, 105-113.

[3] a) G. Kresse, J. Furthmuller, *Phys. Rev. B* **1996**, *54*, 11169-11186; b) G. Kresse, J. Hafner, *Phys. Rev. B* **1994**, *49*, 14251-14269.

[4] G. Kresse, D. Joubert, *Phys. Rev. B* **1999**, *59*, 1758-1775.

[5] a) G. Henkelman, H. Jonsson, *J. Chem. Phys.* **2000**, *113*, 9978-9985; b) G. Henkelman, B. P. Uberuaga, H. Jonsson, *J. Chem. Phys.* **2000**, *113*, 9901-9904.

[6] K. Larmier, C. Chizallet, N. Cadran, S. Maury, J. Abboud, A. F. Lamic-Humblot, E. Marceau, H. Lauron-Pernot, *ACS Cat.* **2015**, *5*, 4423-4437.

[7] a) H. Tetrode, *Annalen Der Physik* **1912**, *38*, 434-442; b) O. Sackur, *Annalen Der Physik* **1912**, *40*, 87-106.

[8] A. Roussey, P. Gentile, D. Lafond, E. Martinez, V. Jousseaume, C. Thieuleux, C. Coperet, *J. Mat. Chem. C* **2013**, *1*, 1583-1587.

[9] a) K. L. Fujdala, I. J. Drake, A. T. Bell, T. D. Tilley, *J. Am. Chem. Soc.* **2004**, *126*, 10864-10866; b) T. Tsuda, T. Saegusa, Hashimot.T, *J. Am. Chem. Soc.* **1972**, *94*, 658-659.

[10] a) I. A. Fisher, A. T. Bell, *J. Catal.* **1997**, *172*, 222-237; b) S. Kattel, B. Yan, Y. Yang, J. G. Chen, P. Liu, *The Journal of the American Chemical Society* **2016**, *138*, 12440-12450.